Russian Journal of Earth Sciences Online ISSN: 1681-1208

Structural Stability of Composite Vortices and Its Application to Jupiter's Great Red Spot

E. M. Arakelyan[1], V. V. Zhmur[1,2,3,*], and O. G. Chkhetiani[4]

[1] Moscow Institute of Physics and Technology, Dolgoprudny, Russian Federation
[2] P. P. Shirshov Institute of Oceanology, Russian Academy of Sciences, Moscow, Russian Federation
[3] Peter the Great St. Petersburg Polytechnic University, St. Petersburg, Russian Federation
[4] A. M. Obukhov Institute of Atmospheric Physics, Russian Academy of Sciences, Moscow, Russian Federation
* **Correspondence to:** V. V. Zhmur, zhmur-vladimir@mail.ru

Abstract: Within the framework of a baroclinic quasi-geostrophic model of the atmosphere in the f-plane approximation, the properties of mesoscale vortices with a complex vortex core structure consisting of a set of embedded confocal ellipsoidal vortices are studied. These vortex structures are called one-component, two-component, three-component, and other vortex structures, depending on the number of embedded vortices. Such formations are called composite vortices. Two-component stationary composite vortices were previously studied, and it turned out that they do not undergo a unique transformation (transition) to a one-component vortex. In contrast to the generally accepted definition of structural stability/instability, it is this property that we will call **structural instability**. Here, we will show that a three-component composite vortex is a structurally stable formation upon its transformation into a two-component vortex. The property of structural stability also remains valid for multicomponent composite vortex structures of higher order than a three-component vortex. Thus, in the hierarchy of multicomponent composite vortex structures, the two-component vortex occupies a special place. It is impossible to create a simpler vortex structure from it–a homogeneous vortex–by transforming the geometric dimensions of an embedded internal vortex with continuous changes in all vortex characteristics. A somewhat different two-component composite vortex, composed of a primary stationary vortex and a small, "weak," non-stationary vortex embedded within it, was previously studied. The stability of this formation was demonstrated. The structural stability (in the above sense) of stationary multicomponent vortex structures to similar perturbations is examined, and it is shown that they are also stable. As a fundamental application of the presented theory, an explanation of the properties of a two-component vortex formation–Jupiter's Great Red Spot–is proposed.

Keywords: Jupiter's Great Red Spot, composite vortex, quasi-geostrophic vortex, non-stationary vortex, potential vorticity

Citation: Arakelyan E. M., Zhmur V. V., and Chkhetiani O. G. (2026), Structural Stability of Composite Vortices and Its Application to Jupiter's Great Red Spot, *Russian Journal of Earth Sciences*, 26, ES4002, EDN: BPKSOA, https://doi.org/10.2205/2026es001163

Research Article

Received: July 1, 2026
Accepted: September 8, 2026
Published: September 27, 2026

Copyright: © 2026. The Authors. This article is an open access article distributed under the terms and conditions of the Creative Commons Attribution (CC BY) license (https://creativecommons.org/licenses/by/4.0/).

1. Introduction

Jupiter's Great Red Spot (GRS) is an elliptical anticyclonic vortex located near 22°S latitude and has been observed since the 1660s. The spot's shape (aspect ratio) and dimensions change continuously over time, primarily in the longitude direction [*Sada et al.*, 1996; *Simon et al.*, 2018]. Over time, the spot has become less elongated. For example, from 2009 to 2020, its length decreased from 16,000 to 12,000 km. Its width ranged from 10,000 to 11,000 km. The aspect ratio during this period changed from 1.5 to 1.1. There was also a decrease in the shear velocity, an increase in the westward drift velocity, a decrease in vorticity, and an increase in the Rossby number $Ro = U/(\Omega L)$ from 0.1 to 0.13–0.14. Here, U and L are the characteristic scales of velocity and size, respectively, and $\Omega = 1.76 \times 10^{-4}$ s^{-1} is the rotation frequency. The vertical scale of the spot, based on

the data from gravitational perturbations, is estimated to be 300 km [*Bolton et al.*, 2021] or 500 km [*Meacham*, 1992]. The velocity inside of the spot is on the order of 30–40 m/s, while the western drift velocity is about 3 m/s. The amplitudes of the zonal velocities that spin out the spot reach 100 m/s.

The idea of defining a spot as a large, stable atmospheric vortex sustained by zonal currents was first proposed by G. S. Golitsyn [*Flierl et al.*, 2019]. In [*Larichev and Reznik*, 1976], the possibility of forming a nonlinear isolated vortex on a shear flow in the β-plane was demonstrated. Soliton barotropic solutions as a model of the GRS were considered in [*Beaumont*, 1980; *Liu et al.*, 2012; *McKiver*, 2015; *Petviashvili*, 1980]. Even then (in the 1970s), it became clear that, for models to better match real data, it was necessary to account for baroclinicity, which is undoubtedly present here [*Dowling and Ingersoll*, 1989; *Nezlin*, 1981; *Romanova*, 1980]. The importance of baroclinic effects was also demonstrated in [*Shetty and Marcus*, 2010]. In quasi-geostrophic model simulations, it was found that the mixing of potential vorticity leads to the formation of organized zonal-type flows or large vortices of the GRS and oval types: for a 1.5-layer model [*Bouchet and Sommeria*, 2002], within the framework of single-layer models [*Asay-Davis et al.*, 2009; *Choi et al.*, 2007; *Shetty and Marcus*, 2010], and in the more complex 1.75-layer model [*Flierl*, 1979].

The models discussed above were, in one way or another, vortex structures with the same horizontal size at all levels or layers–a convenient simplification–but in general, the vortex structures here tend to have a three-dimensional structure close to an ellipsoid [*McKiver*, 2015]. Laboratory experiments and simple estimates show that the parameters of an ellipsoidal vortex are interrelated and can reproduce the observed evolution of the GRS dimensions and characteristics [*Harkett et al.*, 2024]. In [*Zhmur et al.*, 2023], the GRS was considered as a stationary baroclinic quasi-geostrophic ellipsoid with a homogeneous distribution of potential vorticity, rotated by a background shear flow. The vertical size of the GRS calculated for this model, as in [*Harkett et al.*, 2024], turned out to be very close to its current estimates. In [*Vasavada et al.*, 1998], within the framework of the anelastic approximation for Jupiter's conditions, several families of vortices were studied, and it was found that vortices with a constant vorticity distribution and shapes close to ellipsoidal converge during evolution to stable structures similar to the GRS and other Jupiter anticyclones. At the same time, vortices with a constant area with respect to height turn out to be unstable and disintegrate.

Accordingly, the GRS is a system that is both non-stationary and characterized by a distribution of potential vorticity that is not entirely uniform, not only on small scales but also on its main dimensions. The division of the GRS into two regions–an inner core and an outer ring or belt with counter-rotating motion–has been observed for quite some time. The outer region is in intense anticyclonic rotation. Meanwhile, in the inner region, both isolated cyclonic features and, overall, cyclonic rotation are observed [*Asay-Davis et al.*, 2009; *Bouchet and Sommeria*, 2002; *Harkett et al.*, 2024; *Kida*, 1981; *Lemasquerier et al.*, 2020; *Meacham et al.*, 1994; *Nakamula et al.*, 2023; *Parisi et al.*, 2021; *Sánchez-Lavega et al.*, 2018].

These cyclonic structures within the nucleus are about 1,500 km in size. Cyclones of 500–600 km in size have also been observed [*Meacham et al.*, 1994]. The central region appears to be elevated above the outer anticyclonic region and exhibits upwelling and outflow of material. The cyclonic rotation of the central region was first demonstrated in [*Sánchez-Lavega et al.*, 2018]. The cyclonic rotation speed reaches 20 m/s, while the maximum anticyclonic rotation speeds are 150 m/s. In addition to the cyclonic structure in the central region, there is also a stable cyclonic ring surrounding the anticyclonic GRS vortex [*Bouchet and Sommeria*, 2002].

In [*Asay-Davis et al.*, 2009; *Kida*, 1981; *Lemasquerier et al.*, 2020; *Nakamula et al.*, 2023; *Parisi et al.*, 2021], in addition to the cyclonic central region, a fairly dynamic picture of vortical and zonal structures, as well as wave effects, was demonstrated.

The hypothesis that the GRS consists of embedded, oppositely vortical structures was first explicitly proposed in [*Parisi et al.*, 2021], where a detailed analysis of variations in velocity fields and potential vorticity inside and outside the spot was performed using data from the Cassini, Galileo, and the Hubble Space Telescope.

In [*Arakelyan et al.*, 2026a], a steady-state model of the GRS was examined in which the outer part of the vortex rotated anticyclonically, while the inner region was in a state of cyclonic rotation. Such a vortex structure with an "embedded" region was named a composite vortex. The vortex regions in [*Arakelyan et al.*, 2026a] were confocal ellipsoids. It should be noted that the energy of a composite vortex exceeds that of a homogeneous stationary vortex without an embedded region. Hereinafter, we will refer to such a vortex as a two-component composite vortex. Accordingly, a vortex structure that is homogeneous in terms of potential vorticity and in which there is no embedded vortex at all will be called a degenerate composite vortex or a homogeneous vortex.

As it turns out, the properties of stationary homogeneous and two-component composite vortices differ qualitatively from one another, and there is no smooth transition of properties from the composite to the homogeneous vortex. We do not take quantitative differences into account here. Indeed, let us imagine that, given a two-component vortex, we attempt to transform it into a single-component vortex by changing the volume of the inner vortex. We will make use of a very important property of a two-component composite vortex: the potential vorticity of both vortices, given their dimensions and the condition of stationarity of their boundaries, is uniquely determined [*Arakelyan et al.*, 2026a]. There are two ways to transform a two-component vortex into a single-component vortex. The first is to reduce the volume of the inner vortex to zero. The second is to increase the size of the inner vortex to match that of the outer vortex. It would seem that in both cases we would obtain a single, homogeneous vortex. However, in the first case, the inner vortex–will have a finite integral potential vorticity. That is, under such a transformation, a singularity in the potential vorticity field that extends to infinity is produced inside the embedded vortex. In the second case, similar singularities of opposite signs arise, but now in both vortices. Furthermore, the energy of such a structure becomes unbounded, whereas the energy of a homogeneous vortex remains finite. Thus, a homogeneous vortex and a two-component vortex are qualitatively different from one another. We will refer to this phenomenon as the structural instability of a two-component vortex relative to a one-component vortex.

This naturally raises the question: Will a similar problem arise when attempting to create a two-component vortex from a three-component vortex by bringing the sizes of the two embedded vortices closer together? Or, in other words, is a three-component vortex structurally stable when transformed into a two-component composite vortex? We can generalize this approach to multicomponent vortex structures consisting of n confocal vortices embedded within one another. Let us denote such a vortex as an n-component composite vortex and pose the following question: Will an n-component composite vortex remain structurally stable when transformed into an $(n-1)$-component composite vortex by merging two inner vortices into a single vortex?

The concept of structural stability differs from that of "ordinary" stability, yet these properties complement one another. Ordinary stability is defined as follows: a weak initial perturbation is introduced into a given structure (in this case, a vortex). If the perturbation intensifies, the structure in question is considered unstable with respect to that perturbation. In nature, it should not exist or can exist only for a finite time. In this case, the initial form either collapses or transforms into another form. If, however, the initial perturbation remains completely or nearly unchanged, then such a structure is considered stable, and its existence in nature is possible.

In this study, we investigate the stability of composite vortices against weak perturbations in the form of small vortices embedded in one of the constituent regions of this structure. For a homogeneous stationary vortex, such a problem was formulated in [*Arakelyan et al.*, 2026b], where the stability of the specified vortex with respect to a weak perturbation in the form of a small vortex was demonstrated. For two-, three-, and multi-component stationary vortex structures, a similar problem has not been considered previously. Here, we discuss this problem for the first time.

The usual instability can be viewed as the initial stage in the formation of a two-component composite vortex structure from a homogeneous vortex. Similarly, a two-component structure can evolve into a three-component one, and so on. In the case of instability, the energy of a weak perturbation vortex will increase at the energy of the main motion and may lead to a new steady state. In the case of stability, the initially weak perturbation cannot acquire additional energy on its own; however, if energy is somehow "pumped" into the perturbing vortex, the process of forming a two-component vortex system from a homogeneous vortex becomes potentially possible. Under Jupiter's conditions, such an additional energy source exists–namely, the chemical reaction between ammonia and acetylene under the influence of solar ultraviolet radiation, which releases heat and produces reddish-brown compounds. Of course, in this scenario, we would have to abandon the assumption of stationarity for a small, low-intensity vortex.

The objective of this study is to demonstrate the structural stability of a three-component composite vortex and the possibility of transforming it into a two-component vortex structure with a smooth evolution of all physical properties. Arguments are presented in favor of the structural stability of multicomponent composite vortices when they are transformed into composite vortices with one fewer embedded vortex per unit. The vortex's stability against weak perturbations in the form of small vortices inserted into an arbitrary region of the multicomponent vortex structure will also be demonstrated.

It should also be noted that all physical parameters of such a vortex system change continuously during the transformation. Two-component composite vortices play a special role in this approach. They can be created from multi-component composite vortices when pairs of internal vortices merge into a single vortex, with the parameters of these structures evolving continuously. However, this property is limited to two-component composite vortices. Two-component vortices themselves cannot be transformed into single-component vortex systems without a sudden change in their properties. Interestingly, it is precisely the two-component vortex that represents a good approximation for the GRS model.

2. Statement of the Problem

Consider a rotating, density-stratified medium with a constant Brunt–Väisälä frequency. In the quasi-geostrophic approximation (for small Rossby numbers), the equations of motion for an incompressible fluid reduce to a single equation for either the pressure or the stream function, linked by a constant multiplier. In this study, we will use the equation for the stream function $\psi(x, y, z, t)$:

$$\frac{\partial}{\partial t}\left(\Delta_h \psi + \frac{\partial}{\partial z}\frac{f^2}{N^2}\frac{\partial \psi}{\partial z}\right) + J_h\left(\psi, \Delta_h \psi + \frac{\partial}{\partial z}\frac{f^2}{N^2}\frac{\partial \psi}{\partial z}\right) = 0. \tag{1}$$

Here, (x, y) are the horizontal coordinates; z is the vertical coordinate; t is time; $N = \text{const}$ is the Brunt–Väisälä frequency; $f = \text{const}$ is the Coriolis parameter; $\Delta_h = \frac{\partial^2}{\partial x^2} + \frac{\partial^2}{\partial y^2}$ is the Laplace operator with respect to the horizontal coordinates; $J_h(A, B) = \frac{\partial A}{\partial x}\frac{\partial B}{\partial y} - \frac{\partial A}{\partial y}\frac{\partial B}{\partial x}$ is the Jacobian determinant. The velocity field (u, v, w) is expressed in terms of the stream function by the relations:

$$u = -\frac{\partial \psi}{\partial y}, \quad v = \frac{\partial \psi}{\partial x}, \quad w = -\frac{f}{N^2}\left[\frac{\partial^2 \psi}{\partial t \partial z} + J_h\left(\psi, \frac{\partial \psi}{\partial z}\right)\right]. \tag{2}$$

Equation (1), as well as relations (2), is derived with an error of the order of the Rossby number $Ro \ll 1$. From Equation (1), only the geostrophic component of motion can be obtained. Non-geostrophic motions, under this approach, fall under the next Rossby number approximation and are not considered here.

The physical interpretation of Equation (1) reduces to the following: during motion, the magnitude of the potential vorticity for moving fluid particles,

$$\sigma = \Delta_h \psi + \frac{\partial}{\partial z}\frac{f^2}{N^2}\frac{\partial \psi}{\partial z}, \tag{3}$$

is conserved, i.e., σ is a Lagrangian invariant.

The Lagrangian invariant σ, given by Equation (3), is also written here with an accuracy of the Rossby number. It should be noted that $\Delta_h \psi = \mathrm{rot}_z \overrightarrow{u}$, so:

$$\sigma = \mathrm{rot}_z \overrightarrow{u} + \frac{\partial}{\partial z}\frac{f^2}{N^2}\frac{\partial \psi}{\partial z}. \tag{3a}$$

When N and f are constant, Equation (3) can be simplified by introducing a "stretched" vertical coordinate $\tilde{z} = \frac{N}{f} z$. Here, $\frac{N}{f}$ is the stretching factor. Then $\frac{\partial}{\partial z}\frac{f^2}{N^2}\frac{\partial \psi}{\partial z} = \frac{\partial^2 \psi}{\partial \tilde{z}^2}$. And the potential vorticity of the particles can be expressed in terms of the three-dimensional Laplacian in the vertically stretched space $(x, y, \tilde{z})$:

$$\sigma = \Delta \psi = \frac{\partial^2 \psi}{\partial x^2} + \frac{\partial^2 \psi}{\partial y^2} + \frac{\partial^2 \psi}{\partial \tilde{z}^2}. \tag{4}$$

Equation (4) describes the instantaneous distribution of potential vorticity in space. Its usefulness is limited to cases where the distribution is piecewise constant. In particular, the following case has been studied in [*Marcus*, 1988; *Zhmur and Pankratov*, 1989; *Zhmur and Shchepetkin*, 1991]:

$$\Delta \psi = \begin{cases} \sigma_{\mathrm{in}}, \text{ if } (x, y, \tilde{z}) \in V \\ \sigma_{\mathrm{out}}, \text{ if } (x, y, \tilde{z}) \notin V \end{cases}. \tag{5}$$

Here, σ_{in} and σ_{out} are constant quantities, and V is a closed region of the vortex core in the $(x, y, \tilde{z})$ space. The core V can deform and move. σ_{in} is the potential vorticity of particles inside the core, and σ_{out} is the potential vorticity of particles outside the core. In the absence of a vortex, a uniform distribution of potential vorticity is observed throughout space:

$$\Delta \psi = \sigma_{\mathrm{out}}. \tag{6}$$

This relationship defines the background flow. In our approach, the background flow is an isovortical flow. Another possible case is a background fluid simply at rest at infinity with $\sigma_{\mathrm{out}} = 0$. From Equation (6), the solution to the equation $\psi = \psi_f(x, y, \tilde{z})$ represents the flux function of the background flow. We will specify the background flow, so we will consider $\psi_f(x, y, \tilde{z})$ to be a known function.

In the studies mentioned [*Marcus*, 1988; *Zhmur and Pankratov*, 1989; *Zhmur and Shchepetkin*, 1991], an ellipsoid was chosen as the shape of the vortex core V. The background flow was a barotropic, isovortical flow in [*Zhmur and Pankratov*, 1989]. In [*Zhmur and Shchepetkin*, 1991], a baroclinic horizontal flow with a constant vertical shear was considered as the background flow. In all cases, the nature of the background flow determined the value of σ_{out}.

The deviation from the background flow caused by the presence of a vortex is represented by the vorticity function ψ_v for which the following distribution holds:

$$\Delta \psi_v = \begin{cases} (\sigma_{\mathrm{in}} - \sigma_{\mathrm{out}}), \text{ if } (x, y, \tilde{z}) \in V \\ 0, \text{ if } (x, y, \tilde{z}) \notin V \end{cases}, \tag{7}$$

and the general stream function for Equation (5) is written as follows:

$$\psi = \psi_f + \psi_v. \tag{8}$$

Equation (7) is solved in the general case for any shape of the kernel V in the space $(x, y, \tilde{z})$:

$$\psi_v(x, y, \tilde{z}, t) = -\frac{\sigma}{4\pi} \iiint_V \frac{\mathrm{d}x'\mathrm{d}y'\mathrm{d}\tilde{z}'}{\sqrt{(x-x')^2 + (y-y')^2 + (\tilde{z}-\tilde{z}')^2}}. \tag{9a}$$

In this case, the shape of the V-core may depend on time as a parameter. $\sigma = \sigma_{\text{in}} - \sigma_{\text{out}} = \text{const}$–the excess of the potential vorticity of the core particles over that of the background flow particles. An important property of the solution to Equation (9a)–the continuity of the function $\psi_v(x, y, \tilde{z}, t)$ itself and its first spatial derivatives – follows from the theory of the gravitational potential [*Tikhonov and Samarskii*, 1977]. The continuity of the derivatives is equivalent to the continuity of the field of horizontal geostrophic velocities, whereas the continuity of the stream function is equivalent to the continuity of the pressure field. At the boundary of region V (the boundary of the vortex core), the second spatial derivatives are discontinuous, which leads to a discontinuity in the angular velocity field at the vortex boundary. However, the pressure field remains continuous under any deformation of the vortex core. Therefore, the dynamic boundary condition on the surface of the vortex core is automatically satisfied for any current shape and deformation of the vortex core. Meanwhile, the kinematic condition requires additional constraints on the behavior of vortices.

Using Equations (2) and (9a), we can obtain the components of the geostrophic velocities:

$$u_v = \frac{-\partial\psi_v}{\partial y} = \frac{\sigma}{4\pi} \iiint_V \frac{(y-y')\mathrm{d}x'\mathrm{d}y'\mathrm{d}\tilde{z}'}{[(x-x')^2 + (y-y')^2 + (\tilde{z}-\tilde{z}')^2]^{3/2}}, \tag{9b}$$

$$v_v = \frac{\partial\psi_v}{\partial x} = \frac{-\sigma}{4\pi} \iiint_V \frac{(x-x')\mathrm{d}x'\mathrm{d}y'\mathrm{d}\tilde{z}'}{[(x-x')^2 + (y-y')^2 + (\tilde{z}-\tilde{z}')^2]^{3/2}}. \tag{9c}$$

Equations (9b) and (9c) hold for an arbitrary kernel shape. However, the integrals appearing there are generally not evaluated, except in a few special cases, the most general of which is a kernel shaped like an ellipsoid. This problem was solved in the cited studies [*Marcus*, 1988; *Zhmur and Pankratov*, 1989; *Zhmur and Shchepetkin*, 1991]. In particular, for a barotropic background flow or its absence, the aforementioned works derived an expression for $\psi_v(x, y, \tilde{z}, t)$ in the case where the two main directions of the ellipsoid lie in the horizontal plane, and the third main direction is vertical:

$$\psi_v(x, y, \tilde{z}, t) = \frac{-1}{4}\sigma abc \int_\lambda^\infty \left(1 - \frac{\tilde{x}^2}{a^2+\mu} - \frac{\tilde{y}^2}{b^2+\mu} - \frac{\tilde{z}^2}{\tilde{c}^2+\mu}\right) \frac{\mathrm{d}\mu}{\sqrt{(a^2+\mu)(b^2+\mu)(\tilde{c}^2+\mu)}}. \tag{10}$$

Here, a and b are the horizontal semi-axes of the ellipsoid, c is its vertical semi-axis, $\tilde{c} = \frac{N}{f}c$ is the vertical semi-axis stretched by a factor of $\frac{N}{f}$, $\tilde{x}, \tilde{y}$ are the horizontal coordinate axes aligned with the principal axes of the ellipsoid, and $\tilde{z} = \frac{N}{f}z$ is the vertical axis of the coordinate system stretched by a factor of $\frac{N}{f}$. The lower limit $\lambda(\tilde{x}, \tilde{y}, \tilde{z})$ in integral (9a) is the positive root of the cubic equation:

$$\frac{\tilde{x}^2}{a^2+\lambda} + \frac{\tilde{y}^2}{b^2+\lambda} + \frac{\tilde{z}^2}{\tilde{c}^2+\lambda} = 1. \tag{10a}$$

For the region inside the core up to its boundary, we should set $\lambda = 0$. Equation (10) will remain valid if the semi-axial lengths $a, b, \tilde{c}$, as well as the orientation of the coordinate axes $\tilde{x}, \tilde{y}$ depend on time. This arbitrariness is eliminated if a kinematic condition is imposed on the ellipsoidal boundary of the core in solution (10). We have not yet used it. In particular, applying the kinematic condition to a vortex in an ocean at rest at infinity leads to the following property: the boundary of the vortex core (its shape) will rotate with a constant angular velocity without deformation of the axes about the vertical axis. Against the background of an isovorticity barotropic flow, the vortex moves at the speed of the background flow passing through its center. At the same time, it rotates and becomes

deformed, while remaining an ellipsoid. Details can be found in [*Suetin et al.*, 2023; *Zhmur*, 2011; *Zhmur and Pankratov*, 1989]. These studies also demonstrated that there are only three types of evolution of the vortex core's shape: 1) rotation with limited deformation; 2) nutational oscillations with limited deformation; 3) unrestricted elongation of the vortex core. This issue is described in greatest detail in [*Suetin et al.*, 2023]. It was also shown that there are vortex parameters that remain fixed in the background flow at which the vortex shape neither rotates nor deforms, although particle motion is present within it. This is a so-called stationary vortex.

The horizontal velocity field corresponding to the stream function of the ellipsoidal vortex (10) is shown below in the same coordinates:

$$u_v = \frac{-\sigma}{2} ab\tilde{c} \int_{\lambda}^{\infty} \frac{\mathrm{d}\mu}{(b^2+\mu)\sqrt{(a^2+\mu)(b^2+\mu)(\tilde{c}^2+\mu)}} \tilde{y}, \tag{11a}$$

$$v_v = \frac{\sigma}{2} ab\tilde{c} \int_{\lambda}^{\infty} \frac{\mathrm{d}\mu}{(a^2+\mu)\sqrt{(a^2+\mu)(b^2+\mu)(\tilde{c}^2+\mu)}} \tilde{x}. \tag{11b}$$

Note that inside the vortex core the vortex-induced velocities (11a) and (11b) are linear functions of the horizontal coordinates everywhere up to the boundary $\lambda = 0$. At the same time, the stream function ψ_v, according to Equation (9a), is a quadratic function in those same coordinates. Outside the vortex, $\lambda > 0$, and if we are on the surface $\lambda = \text{const} > 0$, the property of linearity of the velocity field with respect to the horizontal coordinates is preserved. Similarly, on this surface, the stream function ψ_v is also a quadratic function. Let us answer the question: "What exactly is the surface $\lambda = \text{const} > 0$?" Let us return to Equation (10). It is clear that the surface $\lambda = \text{const} > 0$ corresponds to the surface of an ellipsoid with semi-axes $(A, B, \tilde{C})$, where $A^2 = a^2 + \lambda$, $B^2 = b^2 + \lambda$, and $\tilde{C}^2 = \tilde{c}^2 + \lambda$. That is, the original ellipsoid with semi-axes $(a, b, \tilde{c})$ lies inside the new ellipsoid with semi-axes $(A, B, \tilde{C})$ and the principal directions of both ellipsoids coincide; most importantly, their foci also coincide. In other words, the two ellipsoids under consideration, with the property $\lambda = \text{const}$, are confocal. When $\lambda = \text{const} < 0$, the ellipsoid with semi-axes $(A, B, \tilde{C})$ lies inside the ellipsoid with semi-axes $(a, b, \tilde{c})$. The following property characterizes the confocality of ellipsoids: the difference of the squares of the distances between the surfaces of the ellipsoids along all three main directions is zero, due to the equality $\lambda = A^2 - a^2 = B^2 - b^2 = \tilde{C}^2 - \tilde{c}^2$.

On timescales of a few Earth years, Jupiter's Great Red Spot can be viewed as a vortex with a frozen core against the background of a barotropic horizontal current with a shear. Short timescales refer to the characteristic rotation period of a particle within the vortex. Long timescales refer to the time scale over which the vortex core is deformed. Over more than 350 years of observations of the GRS, the vortex has slowly deformed, decreasing in size and becoming less elongated. On timescales of the order of one Earth year, the deformation can be neglected, and the vortex can be considered stationary. The GRS was studied in this context in [*Suetin et al.*, 2023], where it was assumed that the vortex core is filled with particles of equal vorticity (in the sense of potential vorticity).

To the present time, two GRS models have been developed in the form of a three-dimensional baroclinic vortex: a vortex with homogeneous potential vorticity in the vortex core [*Suetin et al.*, 2023] and a composite vortex consisting of two embedded homogeneous vortices [*Arakelyan et al.*, 2026a]. The second variant more accurately describes the properties of the GRS. From a mathematical point of view, the second problem can be regarded as an investigation of the structural reorganization of a homogeneous vortex formation when a second vortex is introduced into it, under the condition that the entire vortex system remains stationary. As it turns out, in this case, the homogeneous vortex undergoes significant structural reorganization not only quantitatively but also qualitatively. In other words, the properties of the resulting two-component vortex change significantly

compared to those of the initial homogeneous vortex. The main difference is as follows: the embedded inner vortex rotates the particles in the opposite direction compared to the initial vortex. As a result, the steady-state two-component vortex consists of an inner region with cyclonic motion and a peripheral region with intense anticyclonic rotation of the particles. The volume-averaged motion is anticyclonic. A comparison of the two models raises the question: how will the properties of a two-component vortex change if a third vortex is placed inside it while keeping the stationarity condition in effect? In fact, this problem is equivalent to studying the structural reorganization of a two-component vortex in response to a perturbation by a third vortex.

Let us now modify our approach. Suppose that the core of the vortex consists of three embedded vortices with the following values of potential vorticity. Namely: σ_1 – the outer, large vortex, σ_2 – the inner, medium-sized vortex. Let us call σ_1 the intrinsic potential vorticity of the outer or main vortex. Similarly, let us call σ_2 the intrinsic potential vorticity of the embedded medium-sized vortex. Finally, σ_3 is the intrinsic potential vorticity of the smallest embedded vortex. All three vortices are embedded within one another and simultaneously reside in the background flow with potential vorticity σ_f. Let V_1 denote the set of points occupied by the core of the large vortex; V_2 denote the corresponding set of points of the core of the medium-sized embedded vortex. Finally, V_3 denotes the set of points of the core of the smallest embedded vortex. Recall that the set V_2 is entirely contained within the set V_1, and the set V_3 is contained within V_2: $V_3 \subset V_2 \subset V_1$. Let us denote the gap between the surfaces of the middle inner and outer ellipsoids as $V_1 \cap V_2$. We will denote the analogous gap between the middle and smallest vortices as $V_2 \cap V_3$. As a result, we obtain the following distribution of potential vorticity in space (Figure 1):

$$\sigma = \begin{cases} (\sigma_1 + \sigma_2 + \sigma_3 + \sigma_f), \text{ if the point } (x, y, \tilde{z}) \text{ falls within the region } V_3 \\ (\sigma_1 + \sigma_2 + \sigma_f), \text{ if the point } (x, y, \tilde{z}) \text{ falls within the region } V_2 \cap V_3 \\ (\sigma_1 + \sigma_f), \text{ if the point } (x, y, \tilde{z}) \text{ falls within the region } V_1 \cap V_2 \\ \sigma_f, \text{ if the point } (x, y, \tilde{z}) \text{ lies outside the region } V_1 \end{cases}. \quad (12)$$

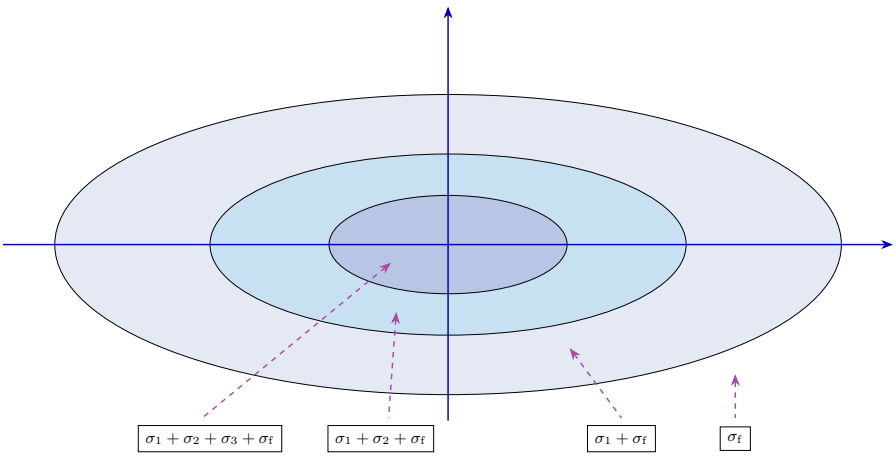


Figure 1. Schematic diagram of a composite vortex structure consisting of three vortices. The outer vortex (the largest) No. 1 occupies region V_1. The intermediate-sized vortex No. 2 occupies region V_2. The smallest inner vortex No. 3 occupies region V_3. In the inner vortex within region V_3, the total potential vorticity of the particles is $(\sigma_1 + \sigma_2 + \sigma_3 + \sigma_f)$. In the gap between the boundaries of vortices No. 3 and No. 2 within region $V_2 \cap V_3$, the potential vorticity of the particles is $(\sigma_1 + \sigma_2 + \sigma_f)$. In the gap between the boundaries of vortices No. 2 and No. 1 in the region $V_1 \cap V_2$, the potential vorticity of the particles is $(\sigma_1 + \sigma_f)$. Finally, outside the region V_1, the potential vorticity of the particles takes on the background value σ_f.

We emphasize that the mathematical space $(x, y, \tilde{z})$ under consideration is stretched vertically by a factor of $\frac{N}{f}$ compared to ordinary physical space (x, y, z). Hereinafter, we will use system (12) as the mathematical formulation of the problem, in which we are required to determine the stream function $\psi(x, y, \tilde{z})$ throughout the entire space.

The directions of the horizontal axes (x, y) have been chosen to coincide with the directions of the principal axes of the ellipsoids. Note that the formulation of Equation (12) does not require the nuclei to have an ellipsoidal shape and is suitable for any simply connected and nested volumes as vortex nuclei. We will use this property later.

3. Solution to the Problem

Based on the linearity of Equation (12), we will decompose the problem into three components $\psi = \psi_f + \psi_1 + \psi_2 + \psi_3$, where ψ_f describes the background flow and obeys Equation (6) throughout the entire space $\Delta\psi_f = \sigma_{\text{out}}$. We will set the background flow.

The stream function ψ_1 describes a large vortex and is governed by the equation:

$$\Delta\psi_1 = \begin{cases} \sigma_1, \text{ if } (x, y, \tilde{z}) \in V_1 \\ 0, \text{ if } (x, y, \tilde{z}) \notin V_1 \end{cases}. \tag{13}$$

The potential vorticity σ_1 is the intrinsic potential vorticity of vortex No. 1. For the ellipsoidal shape of the core $F_1(x, y, \tilde{z}) = \frac{x^2}{a_1^2} + \frac{y^2}{b_1^2} + \frac{\tilde{z}^2}{\tilde{c}_1^2} - 1 = 0$ and for any point in space $(x, y, \tilde{z})$, the following solution follows from Equation (9a):

$$\psi_1(x, y, \tilde{z}, t) = -\frac{1}{4}\sigma_1 a_1 b_1 \tilde{c}_1 \int_{\lambda_1}^{\infty} \left(1 - \frac{x^2}{a_1^2 + \mu} - \frac{y^2}{b_1^2 + \mu} - \frac{\tilde{z}^2}{\tilde{c}_1^2 + \mu}\right) \times \frac{\mathrm{d}\mu}{\sqrt{(a_1^2 + \mu)(b_1^2 + \mu)(\tilde{c}_1^2 + \mu)}}.$$

The region V_1 in (13) is the core of the main vortex.The lower limit of integration for the parameter λ_1 for the space inside the region V_1 is zero: $\lambda_1 = 0$. For points outside V_1, λ_1 is defined as follows: a chosen external point $(x, y, \tilde{z})$ lies on the surface of one of the outside confocal ellipsoids, to which $\lambda_1 > 0$ corresponds, satisfying the equation:

$$\frac{x^2}{a_1^2 + \lambda_1} + \frac{y^2}{b_1^2 + \lambda_1} + \frac{\tilde{z}^2}{\tilde{c}_1^2 + \lambda_1} = 1.$$

ψ_2 describes the average embedded vortex and obeys an equation analogous to Equation (13):

$$\Delta\psi_2 = \begin{cases} \sigma_2, \text{ if } (x, y, \tilde{z}) \in V_2 \\ 0, \text{ if } (x, y, \tilde{z}) \notin V_2 \end{cases}. \tag{14}$$

Solution (14) fully repeats the considerations for a large vortex, the solution for which is presented below:

$$\psi_2(x, y, \tilde{z}, t) = -\frac{1}{4}\sigma_2 a_2 b_2 \tilde{c}_2 \int_{\lambda_2}^{\infty} \left(1 - \frac{x^2}{a_2^2 + \mu} - \frac{y^2}{b_2^2 + \mu} - \frac{\tilde{z}^2}{\tilde{c}_2^2 + \mu}\right) \frac{\mathrm{d}\mu}{\sqrt{(a_2^2 + \mu)(b_2^2 + \mu)(\tilde{c}_2^2 + \mu)}}.$$

Similarly, σ_2 is the intrinsic vortex potential of vortex No. 2. As with the first vortex, the parameter λ_2 is zero for points inside the region V_2: $\lambda_2 = 0$. For points outside V_2, λ_2 is determined in a similar manner: the chosen external point $(x, y, \tilde{z})$ lies on the surface of one of the confocal ellipsoids, to which $\lambda_2 > 0$ corresponds, and which satisfies the equation:

$$\frac{x^2}{a_2^2 + \lambda_2} + \frac{y^2}{b_2^2 + \lambda_2} + \frac{\tilde{z}^2}{\tilde{c}_2^2 + \lambda_2} = 1.$$

Similarly, for ψ_3, we have the distribution of potential vorticity:

$$\Delta\psi_3 = \begin{cases} \sigma_3, \text{ if } (x,y,\tilde{z}) \in V_3 \\ 0, \text{ if } (x,y,\tilde{z}) \notin V_3 \end{cases}. \tag{15}$$

Solution (15) is analogous to the formula for $\psi_2(x,y,\tilde{z},t)$, where the subscript 2 must be substituted with 3. As all the ellipsoids under consideration are confocal, for any point in space chosen outside the vortex, λ_1, λ_2, and λ_3 are related by the following equations:

$$a_1^2+\lambda_1 = a_2^2+\lambda_2 = a_3^2+\lambda_3, \quad b_1^2+\lambda_1 = b_2^2+\lambda_2 = b_3^2+\lambda_3, \quad \tilde{c}_1^2+\lambda_1 = \tilde{c}_2^2+\lambda_2 = \tilde{c}_3^2+\lambda_3.$$

Since the outer ellipsoid is larger than the inner one, that is, $a_1 > a_2 > a_3$, $b_1 > b_2 > b_3$ and $\tilde{c}_1 > \tilde{c}_2 > \tilde{c}_3$, then $\lambda_3 > \lambda_2 > \lambda_1$.

The velocity fields induced by vortex No. 1 (outer), No. 2 (middle inner), and No. 3 (smallest inner) can also be easily calculated.

For convenience, let us introduce some additional notation:

$$\alpha_0 = ab\tilde{c}\int_0^\infty \frac{\mathrm{d}\mu}{(a^2+\mu)\sqrt{(a^2+\mu)(b^2+\mu)(\tilde{c}^2+\mu)}} = K\int_0^\infty \frac{\mathrm{d}\mu}{(\varepsilon+\mu)\sqrt{(\varepsilon+\mu)(\varepsilon^{-1}+\mu)(K^2+\mu)}}, \tag{16a}$$

$$\beta_0 = ab\tilde{c}\int_0^\infty \frac{\mathrm{d}\mu}{(b^2+\mu)\sqrt{(a^2+\mu)(b^2+\mu)(\tilde{c}^2+\mu)}} = K\int_0^\infty \frac{\mathrm{d}\mu}{(\varepsilon^{-1}+\mu)\sqrt{(\varepsilon+\mu)(\varepsilon^{-1}+\mu)(K^2+\mu)}}, \tag{16b}$$

$$\alpha_\lambda = ab\tilde{c}\int_\lambda^\infty \frac{\mathrm{d}\mu}{(a^2+\mu)\sqrt{(a^2+\mu)(b^2+\mu)(\tilde{c}^2+\mu)}} = K\int_{\lambda'}^\infty \frac{\mathrm{d}\mu}{(\varepsilon+\mu)\sqrt{(\varepsilon+\mu)(\varepsilon^{-1}+\mu)(K^2+\mu)}}, \tag{16c}$$

$$\beta_\lambda = ab\tilde{c}\int_\lambda^\infty \frac{\mathrm{d}\mu}{(b^2+\mu)\sqrt{(a^2+\mu)(b^2+\mu)(\tilde{c}^2+\mu)}} = K\int_{\lambda'}^\infty \frac{\mathrm{d}\mu}{(\varepsilon^{-1}+\mu)\sqrt{(\varepsilon+\mu)(\varepsilon^{-1}+\mu)(K^2+\mu)}}. \tag{16d}$$

All of the functions listed are dimensionless. However, calculations can be performed in both dimensional and dimensionless forms. Here we present both forms–dimensional and dimensionless. The left column of Equations (16a)–(16d) is the dimensional form, and the right column is the dimensionless form. New dimensionless parameters of the vortex have appeared here. $\varepsilon = \frac{a}{b}$ is the horizontal elongation parameter, and $K = \frac{\tilde{c}}{\sqrt{ab}}$ is the vertical elongation parameter of the vortex core. In addition, the dimensionless lower limit $\lambda' = \frac{\lambda}{ab}$ has appeared in the dimensionless form; this is the positive root of the dimensionless Equation (10a):

$$\frac{x'^2}{\varepsilon+\lambda'} + \frac{y'^2}{\varepsilon^{-1}+\lambda'} + \frac{\tilde{z}'^2}{K^2+\lambda'} = 1, \quad \text{where } (x',y',\tilde{z}') = \frac{(x,y,\tilde{z})}{\sqrt{ab}}.$$

Here, $(x', y', \tilde{z}')$ are the dimensionless coordinates of the point $(x, y, \tilde{z})$. In terms of the functions (16a)–(16d), the velocity field is written as (the dimensional form of notation is convenient here):

$$u = -\frac{1}{2}\sigma\beta_\lambda y, \quad v = \frac{1}{2}\sigma\alpha_\lambda x.$$

In the GRS, the vortex is elongated in the east-west direction along a parallel. Therefore, it is convenient to orient the x-axis toward the east and the y-axis toward the north. These will also be the main directions of all ellipsoids. With this choice of coordinates, the background flow–in the form of a horizontal barotropic flow with a shear–is described by the following relations:

$$\begin{cases} u_f = -\Gamma y, \\ v_f = 0. \end{cases}$$

Since we have three vortices, the relations must be numbered for each vortex. For vortex No. 1 with semi-axes $(a_1, b_1, \tilde{c}_1)$, potential vorticity σ_1 and boundary equation $F_1(x, y, \tilde{z}) = \frac{x^2}{a_1^2} + \frac{y^2}{b_1^2} + \frac{\tilde{z}^2}{\tilde{c}_1^2} - 1 = 0$, we denote the parameters $\alpha_0, \beta_0, \alpha_\lambda$ and β_λ as $\alpha_0^{(1)}, \beta_0^{(1)}, \alpha_{\lambda_1}^{(1)}$ and $\beta_{\lambda_1}^{(1)}$. Similarly, for vortex No. 2 with semi-axes $(a_2, b_2, \tilde{c}_2)$, potential vorticity σ_2 and boundary equation $F_2(x, y, \tilde{z}) = \frac{x^2}{a_2^2} + \frac{y^2}{b_2^2} + \frac{\tilde{z}^2}{\tilde{c}_2^2} - 1 = 0$, we introduce the notation $\alpha_0^{(2)}, \beta_0^{(2)}, \alpha_{\lambda_2}^{(2)}, \beta_{\lambda_2}^{(2)}$. Finally, for vortex No. 3, we use the notations $\alpha_0^{(3)}, \beta_0^{(3)}, \alpha_{\lambda_3}^{(3)}$ and $\beta_{\lambda_3}^{(3)}$. In this case, it is more convenient to use dimensional relations.

As a result, the velocity field at the boundary of outer core No. 1 will be the sum of the flows from four sources–the background flow and the flows from the three vortices. The flow induced by vortex No. 1 is shown below:

$$u_1 = -\frac{1}{2}\sigma_1\beta_0^{(1)} y, \quad v_1 = \frac{1}{2}\sigma_1\alpha_0^{(1)} x. \tag{17}$$

Now let us move on to vortex No. 2. The induced flow from vortex No. 2 at the boundary of core No. 1 is located in a region outside core No. 2, so the velocities here are more complicated:

$$u_2 = -\frac{1}{2}\sigma_2\beta_{\lambda_{21}}^{(2)} y, \quad v_2 = \frac{1}{2}\sigma_2\alpha_{\lambda_{21}}^{(2)} x. \tag{18}$$

For convenience, we have introduced the parameter $\lambda_{21} = a_1^2 - a_2^2 = b_1^2 - b_2^2 = \tilde{c}_1^2 - \tilde{c}_2^2$, which has the same physical meaning but uses more intuitive indices.

Ultimately, the flow from vortex No. 3, also in the region outside of core No. 3 at the boundary of the first vortex, is induced by the following velocities:

$$u_3 = -\frac{1}{2}\sigma_3\beta_{\lambda_{31}}^{(3)} y, \quad v_3 = \frac{1}{2}\sigma_3\alpha_{\lambda_{31}}^{(3)} x. \tag{19}$$

Here, similarly, we define $\lambda_{31} = a_1^2 - a_3^2 = b_1^2 - b_3^2 = \tilde{c}_1^2 - \tilde{c}_3^2$.

The velocities (17), (18), and (19) are linear functions in the coordinates at the boundary of vortex No. 1 due to the property of joint focusing of all vortices.

The final total components of velocity at the boundary of the large vortex (vortex No. 1) are also linear functions in the horizontal coordinates:

$$\begin{aligned} u &= u_f + u_1 + u_2 + u_3 = -\left(\Gamma + \frac{1}{2}\sigma_1\beta_0^{(1)} + \frac{1}{2}\sigma_2\beta_{\lambda_{21}}^{(2)} + \frac{1}{2}\sigma_3\beta_{\lambda_{31}}^{(3)}\right) y, \\ v &= v_f + v_1 + v_2 + v_3 = \left(\frac{1}{2}\sigma_1\alpha_0^{(1)} + \frac{1}{2}\sigma_2\alpha_{\lambda_{21}}^{(2)} + \frac{1}{2}\sigma_3\alpha_{\lambda_{31}}^{(3)}\right) x. \end{aligned} \tag{20}$$

The coordinates (x, y) are variables and correspond to the boundary of vortex core No. 1. Note that the given relations (20) satisfy the basic Equation (1) and the dynamic

condition at the boundary of the outer core. However, they do not yet satisfy the kinematic condition at this same boundary.

We write the boundary equation for vortex No. 1 in general form as $F_1(x,y,z,t)=0$. Then the kinematic condition preventing fluid particles from flowing through the boundary can be written as:

$$\frac{\partial F_1}{\partial t}+u\frac{\partial F_1}{\partial x}+v\frac{\partial F_1}{\partial y}+w\frac{\partial F_1}{\partial z}=0. \tag{21}$$

Moreover, the term $w\frac{\partial F_1}{\partial z}$ in this equation is small in comparison with the terms $u\frac{\partial F_1}{\partial x}$ and $v\frac{\partial F_1}{\partial y}$. The ratio of $w\frac{\partial F_1}{\partial z}$ to the aforementioned terms of Equation (21) is of the order of the Rossby number $Ro\ll 1$ and should be considered an insignificant addition to the simplified boundary condition:

$$\frac{\partial F_1}{\partial t}+u\frac{\partial F_1}{\partial x}+v\frac{\partial F_1}{\partial y}=0. \tag{22}$$

With this kinematic condition (22), all equations of the problem are written with the same accuracy up to terms of the order $Ro\ll 1$. Now let us concretize the boundary equation $F_1(x,y,\tilde{z},t)=0$:

$$F_1(x,y,\tilde{z})=\frac{x^2}{a_1^2}+\frac{y^2}{b_1^2}+\frac{\tilde{z}^2}{\tilde{c}_1^2}-1=0.$$

Let us assume–and this is a very important assumption–that this boundary is stationary, i.e., independent of time t. Given the relations $\frac{\partial F_1}{\partial t}=0$, $\frac{\partial F_1}{\partial x}=\frac{2x}{a_1^2}$, $\frac{\partial F_1}{\partial y}=\frac{2y}{b_1^2}$, and using Equations (20), we obtain the kinematic condition:

$$\left\{\frac{1}{a_1^2}\left(2\Gamma+\sigma_1\beta_0^{(1)}+\sigma_2\beta_{\lambda_{21}}^{(2)}+\sigma_3\beta_{\lambda_{31}}^{(3)}\right)+\frac{1}{b_1^2}\left(\sigma_1\alpha_0^{(1)}+\sigma_2\alpha_{\lambda_{21}}^{(2)}+\sigma_3\alpha_{\lambda_{31}}^{(3)}\right)\right\}xy=0. \tag{23}$$

In the Equation (23) the coordinates (x,y) are variable and correspond to the coordinates of the boundary of outer vortex No. 1. In this case, the kinematic condition on the boundary of vortex No. 1 is the relation:

$$\frac{-1}{a_1^2}\left(2\Gamma+\sigma_1\beta_0^{(1)}+\sigma_2\beta_{\lambda_{21}}^{(2)}+\sigma_3\beta_{\lambda_{31}}^{(3)}\right)+\frac{1}{b_1^2}\left(\sigma_1\alpha_0^{(1)}+\sigma_2\alpha_{\lambda_{21}}^{(2)}+\sigma_3\alpha_{\lambda_{31}}^{(3)}\right)=0, \tag{24}$$

or in a more convenient representation:

$$\sigma_1\left(\frac{-\beta_0^{(1)}}{a_1^2}+\frac{\alpha_0^{(1)}}{b_1^2}\right)+\sigma_2\left(\frac{-\beta_{\lambda_{21}}^{(2)}}{a_1^2}+\frac{\alpha_{\lambda_{21}}^{(2)}}{b_1^2}\right)+\sigma_3\left(\frac{-\beta_{\lambda_{31}}^{(3)}}{a_1^2}+\frac{\alpha_{\lambda_{31}}^{(3)}}{b_1^2}\right)=\frac{2\Gamma}{a_1^2}. \tag{25}$$

In formulas (24) and (25), the (x,y) coordinates are omitted. Consider the boundary of vortex No. 2. In this case, $\lambda_1=\lambda_2=0$, and $\lambda_{32}=a_2^2-a_3^2=b_2^2-b_3^2=\tilde{c}_2^2-\tilde{c}_3^2>0$. Similar arguments for the boundary of the middle vortex No. 2 yield a relation similar to Equation (25):

$$\sigma_1\left(\frac{-\beta_0^{(1)}}{a_2^2}+\frac{\alpha_0^{(1)}}{b_2^2}\right)+\sigma_2\left(\frac{-\beta_0^{(2)}}{a_2^2}+\frac{\alpha_0^{(2)}}{b_2^2}\right)+\sigma_3\left(\frac{-\beta_{\lambda_{32}}^{(3)}}{a_2^2}+\frac{\alpha_{\lambda_{32}}^{(3)}}{b_2^2}\right)=\frac{2\Gamma}{a_2^2}. \tag{26}$$

For vortex boundary No. 3, where $\lambda_1=\lambda_2=\lambda_3=0$, we obtain a similar equation:

$$\sigma_1\left(\frac{-\beta_0^{(1)}}{a_3^2}+\frac{\alpha_0^{(1)}}{b_3^2}\right)+\sigma_2\left(\frac{-\beta_0^{(2)}}{a_3^2}+\frac{\alpha_0^{(2)}}{b_3^2}\right)+\sigma_3\left(\frac{-\beta_0^{(3)}}{a_3^2}+\frac{\alpha_0^{(3)}}{b_3^2}\right)=\frac{2\Gamma}{a_3^2}. \tag{27}$$

As a result, from the joint kinematic condition (25), (26), and (27) at the three boundaries of the vortices, we can derive a system of equations for the parameters of the vortices:

$$\begin{cases} \sigma_1\left(\dfrac{-\beta_0^{(1)}}{a_1^2}+\dfrac{\alpha_0^{(1)}}{b_1^2}\right)+\sigma_2\left(\dfrac{-\beta_{\lambda_{21}}^{(2)}}{a_1^2}+\dfrac{\alpha_{\lambda_{21}}^{(2)}}{b_1^2}\right)+\sigma_3\left(\dfrac{-\beta_{\lambda_{31}}^{(3)}}{a_1^2}+\dfrac{\alpha_{\lambda_{31}}^{(3)}}{b_1^2}\right)=\dfrac{2\Gamma}{a_1^2}, \\ \sigma_1\left(\dfrac{-\beta_0^{(1)}}{a_2^2}+\dfrac{\alpha_0^{(1)}}{b_2^2}\right)+\sigma_2\left(\dfrac{-\beta_0^{(2)}}{a_2^2}+\dfrac{\alpha_0^{(2)}}{b_2^2}\right)+\sigma_3\left(\dfrac{-\beta_{\lambda_{32}}^{(3)}}{a_2^2}+\dfrac{\alpha_{\lambda_{32}}^{(3)}}{b_2^2}\right)=\dfrac{2\Gamma}{a_2^2}, \\ \sigma_1\left(\dfrac{-\beta_0^{(1)}}{a_3^2}+\dfrac{\alpha_0^{(1)}}{b_3^2}\right)+\sigma_2\left(\dfrac{-\beta_0^{(2)}}{a_3^2}+\dfrac{\alpha_0^{(2)}}{b_3^2}\right)+\sigma_3\left(\dfrac{-\beta_0^{(3)}}{a_3^2}+\dfrac{\alpha_0^{(3)}}{b_3^2}\right)=\dfrac{2\Gamma}{a_3^2}. \end{cases}$$

By introducing the dimensionless potential vorticity of vortices No. 1, No. 2, and No. 3 using the relations $\Gamma_1=\frac{\sigma_1}{\Gamma}$, $\Gamma_2=\frac{\sigma_2}{\Gamma}$, $\Gamma_3=\frac{\sigma_3}{\Gamma}$, the system can be expressed in dimensionless form:

$$\begin{cases} \Gamma_1\left(-\beta_0^{(1)}+\varepsilon_1^2\alpha_0^{(1)}\right)+\Gamma_2\left(-\beta_{\lambda_{21}}^{(2)}+\varepsilon_1^2\alpha_{\lambda_{21}}^{(2)}\right)+\Gamma_3\left(-\beta_{\lambda_{31}}^{(3)}+\varepsilon_1^2\alpha_{\lambda_{31}}^{(3)}\right)=2, \\ \Gamma_1\left(-\beta_0^{(1)}+\varepsilon_2^2\alpha_0^{(1)}\right)+\Gamma_2\left(-\beta_0^{(2)}+\varepsilon_2^2\alpha_0^{(2)}\right)+\Gamma_3\left(-\beta_{\lambda_{32}}^{(3)}+\varepsilon_2^2\alpha_{\lambda_{32}}^{(3)}\right)=2, \\ \Gamma_1\left(-\beta_0^{(1)}+\varepsilon_3^2\alpha_0^{(1)}\right)+\Gamma_2\left(-\beta_0^{(2)}+\varepsilon_3^2\alpha_0^{(2)}\right)+\Gamma_3\left(-\beta_0^{(3)}+\varepsilon_3^2\alpha_0^{(3)}\right)=2. \end{cases} \tag{28}$$

If both internal vortices were completely absent, then the second and third conditions in Equation (28) would not be necessary. If $\Gamma_2=\Gamma_3=0$ then the first equation in Equation (28) yields a solution in the form of the relative vorticity of the main (outer) core:

$$\Gamma_1=\Gamma_1^{(1)}=\frac{2}{-\beta_0^{(1)}+\varepsilon_1^2\alpha_0^{(1)}}, \tag{29}$$

without internal vortices. It is precisely this problem, formulated in a similar way but with a different solution method, that was studied in [*Suetin et al.*, 2023]. We will consider $\Gamma_1^{(1)}$ from Equation (29) as a reference solution against which we will compare the solution to system (28). The solution of Equation (29) represents a stationary homogeneous vortex in a shear flow. The superscript in parentheses (1) in the expression indicates that in this case we are considering a single vortex.

If the inner vortex No. 3 is absent, then the boundary condition at its boundary is also absent, and problem (28) simplifies and reduces to the problem of a stationary composite vortex consisting of two embedded vortices, No. 1 and No. 2. The corresponding system of equations for this situation is given below:

$$\begin{cases} \Gamma_1\left(-\beta_0^{(1)}+\varepsilon_1^2\alpha_0^{(1)}\right)+\Gamma_2\left(-\beta_{\lambda_{21}}^{(2)}+\varepsilon_1^2\alpha_{\lambda_{21}}^{(2)}\right)=2, \\ \Gamma_1\left(-\beta_0^{(1)}+\varepsilon_2^2\alpha_0^{(1)}\right)+\Gamma_2\left(-\beta_0^{(2)}+\varepsilon_2^2\alpha_0^{(2)}\right)=2. \end{cases} \tag{29a}$$

It is specifically this situation that was studied in [*Arakelyan et al.*, 2026a]. Let us denote the solution to this system as $(\Gamma_1^{(2)},\Gamma_2^{(2)})$. The superscript (2) in $\Gamma_1^{(2)},\Gamma_2^{(2)}$ indicates that in this case we are studying a composite vortex consisting of two vortices. As follows from Equation (26), if the geometric parameters of vortices No. 1 and No. 2 are given, then $\Gamma_1^{(2)},\Gamma_2^{(2)}$ are uniquely determined. Cases where the system (29a) has no solutions were not found. However, when the volume of the inner vortex No. 2 was reduced to zero or its dimensions were made to approach those of vortex No. 1, a peculiarity in the behavior of the parameters $(\Gamma_1^{(2)},\Gamma_2^{(2)})$ was observed. However, when the sizes of the vortices were estimated based on measurements from the interplanetary missions Voyager 1 (1979), Galileo (1996), Cassini (2000), or using the Hubble Space Telescope (HST), no peculiarities

in the behavior of the vortices were observed, and the values themselves $(\Gamma_1^{(2)}, \Gamma_2^{(2)})$ for different missions did not differ significantly from one another.

Back to Problem (28). It is natural to expect that system (28) has a unique solution $(\Gamma_1, \Gamma_2, \Gamma_3) = (\Gamma_1^{(3)}, \Gamma_2^{(3)}, \Gamma_3^{(3)})$ for a given geometric configuration of a composite vortex system consisting of three vortices.

It is interesting to compare the vorticity distributions of composite vortices for the cases of two- and three-vortex systems $(\Gamma_1^{(2)}, \Gamma_2^{(2)})$ and $(\Gamma_1^{(3)}, \Gamma_2^{(3)}, \Gamma_3^{(3)})$. The distribution of the total potential vorticity of a two-component composite vortex in dimensionless form is as follows: inside the small vortex: $(1 + \Gamma_1^{(2)} + \Gamma_2^{(2)})$; in the gap between the vortex boundaries $(1 + \Gamma_1^{(2)})$; outside the vortex structure–the background potential vorticity–is one (1).

A similar distribution for a three-component vortex looks like this: inside the small vortex $(1 + \Gamma_1^{(3)} + \Gamma_2^{(3)} + \Gamma_3^{(3)})$, in the gap between the boundaries of the small and medium vortices $(1 + \Gamma_1^{(3)} + \Gamma_2^{(3)})$, and on the peripheral part of the vortex in the gap between the boundaries of the medium and large vortices $(1 + \Gamma_1^{(3)})$. Finally, outside the vortex system, the background potential vorticity is also equal to one.

It should be noted right away that all geometric parameters of the problem have characteristic values of the order of one; therefore, if we fix two vortices in a two-component vortex structure and calculate $(\Gamma_1^{(2)}, \Gamma_2^{(2)})$ according to Equation (29a), and then add a third vortex to the system and calculate $(\Gamma_1^{(3)}, \Gamma_2^{(3)}, \Gamma_3^{(3)})$, then–if the geometric dimensions of the third vortex differ significantly from those of the first two–we will obtain a substantially different picture on a quantitative level.

The addition of a third vortex leads to a significant restructuring of the entire system. It should be noted that we cannot perturb a composite two-component vortex with a weak third vortex, as is done in traditional stability problems. The reason is that an additional condition–stationarity–is imposed on the entire system. It is precisely the stationarity in the kinematic boundary condition (22) that defines the rules and prevents the system from being subjected to arbitrary (including small) perturbations.

If we determine the geometric parameters of the two vortices–the outer and inner ones–and adjust the size of the third vortex so that it roughly matches the size of the inner vortex, it is quite natural to expect that the steady-state distribution of total vortex potential in two-component and three-component composite vortices will be similar. In particular, the potential vorticities of the inner parts of both vortices $(1 + \Gamma_1^{(2)} + \Gamma_2^{(2)})$ and $(1 + \Gamma_1^{(3)} + \Gamma_2^{(3)} + \Gamma_3^{(3)})$ will coincide, and the potential vorticity quantities of the peripheral zones $(1 + \Gamma_1^{(2)})$ and $(1 + \Gamma_1^{(3)})$ of these vortices will also be equal. As for the narrow band between the boundaries of the second and third vortices in a three-component system–which is completely absent in a two-component composite vortex–it is important that the total potential vorticity $(1 + \Gamma_1^{(3)} + \Gamma_2^{(3)})$ in this small gap is limited. In this case, the integral potential vorticity of the region of the specified gap will tend toward zero and will have no effect on the remaining regions of the composite vortex.

3.1. Results of the Numerical Calculation

In each of the space missions–Voyager 1 (1979), Galileo (1996), Cassini (2000)–or using the Hubble Space Telescope (HST), the geometric parameters of the GRS were measured, which were suitable for estimating the parameters of a two-component composite vortex. The major a_1 and minor b_1 dimensions of the primary vortex were determined, as well as the corresponding characteristics (a_2 and b_2) of the embedded vortex. As a result, the dimensionless parameter $\frac{a_2 b_2}{a_1 b_1}$ was determined in each mission. This number varied slightly from mission to mission. The vertical parameter of the main (large) vortex, $K_1 = \frac{\tilde{c}_1}{\sqrt{a_1 b_1}}$, was estimated in [*Suetin et al.*, 2023] and ranged from 4 to 8. For our calculations, we selected three values of K_1 from this range: 4, 6, and 8. From the condition of co-focality, three values of the parameter $K_2 = \frac{\tilde{c}_2}{\sqrt{a_2 b_2}}$ were determined, and with a fixed $\frac{a_2 b_2}{a_1 b_1}$, the dimensions

of the third co-focal vortex were varied via the parameter $M = \frac{a_3 b_3}{a_1 b_1}$ within the range $0 < M < 1$. The vertical parameter of the third vortex, $K_3 = \frac{\tilde{c}_3}{\sqrt{a_3 b_3}}$, was calculated from the co-focality condition. As a result, all necessary coefficients were calculated in system (28), and the dimensionless values $(\Gamma_1^{(3)}, \Gamma_2^{(3)}, \Gamma_3^{(3)})$ of the intrinsic potential vorticities of the vortices in the composite vortex structure were determined, corresponding to a specific K_1 for a variable M.

Figures 2–4 show the calculation results for the following characteristics of composite vortices. The proper potential vorticities of the cores of all three vortices $(\Gamma_1^{(3)}, \Gamma_2^{(3)}, \Gamma_3^{(3)})$ depending on the size of vortex #3, for which the dimensionless parameter $M = \frac{a_3 b_3}{a_1 b_1}$ is chosen, the area of vortex #3 relative to the main vortex #1. This parameter varies in the range of values $0 < M < 1$. In this case, the sizes of vortices #1 and #2 were fixed and taken from the Voyager 1 1979, Galileo 1996, Cassini 2000 missions or using the Hubble Space Telescope (HST, 2006). The red vertical line in these figures corresponds to the situation when vortices #2 and #3 are the same size. Some general properties follow from the figures. Regardless of the value of M, the largest No. 1 and middle vortices are anticyclones (particle rotation is counterclockwise in the southern hemisphere). While the inner vortex is always a cyclonic formation. As follows from the figures, in the vicinity of the coincidence of vortices No. 2 and No. 3 in parameter M, no peculiarities in the behavior of the sets $(\Gamma_1^{(3)}, \Gamma_2^{(3)}, \Gamma_3^{(3)})$ are observed. Conversely, as M approaches 0 or 1, the potential vorticity of the core of vortex #3 has the singularity $\Gamma_3^{(3)} \to -\infty$, as well as $\Gamma_1^{(3)} \to +\infty$ as $M \to 1$. The qualitative behavior of the parameters $(\Gamma_1^{(3)}, \Gamma_2^{(3)}, \Gamma_3^{(3)})$ in a system of three vortices depending on M is generally similar to the behavior of a system of two vortices $(\Gamma_1^{(2)}, \Gamma_2^{(2)})$. The peripheral part rotates particles anticyclonically, the inner zone – cyclonically.

From a physics perspective, the most significant relationships are those between the parameters $(1 + \Gamma_1^{(3)} + \Gamma_2^{(3)} + \Gamma_3^{(3)})$, $(1 + \Gamma_1^{(3)} + \Gamma_2^{(3)})$, $(1 + \Gamma_1^{(3)})$ as functions of M. Note that $(1 + \Gamma_1^{(3)} + \Gamma_2^{(3)} + \Gamma_3^{(3)})$ describes the total potential vorticity of the inner part of the composite vortex (zone V_3), the parameter $(1 + \Gamma_1^{(3)})$ accounts for the total potential vorticity of the peripheral part of the composite vortex (zone $V_1 \cap V_{2,3}$), located between the boundaries of the large vortex No. 1 and the next largest vortex, No. 2 or No. 3. The parameter $(1 + \Gamma_1^{(3)} + \Gamma_2^{(3)})$ is responsible for the total potential vorticity of the intermediate zone $V_2 \cap V_3$ between vortices No. 2 and No. 3. Common properties of the parameters $(1 + \Gamma_1^{(3)} + \Gamma_2^{(3)} + \Gamma_3^{(3)})$ and $(1 + \Gamma_1^{(3)})$ are the cyclonic rotation of particles in the central part of the composite vortex and the anticyclonic rotation in the peripheral zone. These properties are independent of the value of M. The intermediate zone with vorticity $(1 + \Gamma_1^{(3)} + \Gamma_2^{(3)})$ also exhibits anticyclonic rotation throughout its entire extent. The total potential vorticity of this zone becomes singular: $(1 + \Gamma_1^{(3)} + \Gamma_2^{(3)} + \Gamma_3^{(3)}) \to -\infty$ as $M \to 0$, as the size of the smallest vortex, No. 3, decreases. At the opposite end of the interval, as $M \to 1$, the singularities have parameters $(1 + \Gamma_1^{(3)} + \Gamma_2^{(3)})$ and $(1 + \Gamma_1^{(3)})$, which grow unbounded: $(1 + \Gamma_1^{(3)} + \Gamma_2^{(3)}) \to \infty$ and $(1 + \Gamma_1^{(3)}) \to \infty$. In this case, the curves $(1 + \Gamma_1^{(3)} + \Gamma_2^{(3)})$ and $(1 + \Gamma_1^{(3)})$ converge as $M \to 1$.

Thus, two-component and three-component composite vortices exhibit qualitatively identical properties across the entire range of M values. Quantitatively, however, their characteristics differ provided that the inner vortices No. 2 and No. 3 differ significantly in the area they occupy. Nevertheless, when the areas S_2 and S_3 differ only slightly, the central and peripheral zones exhibit identical total potential vorticity for both two-component and three-component composite vortices. Consequently, if a third vortex is placed within a two-component stationary composite vortex–that is, if it is transformed into a three-component stationary vortex structure–the characteristics of the new vortex will be significantly distorted. However, if the third vortex, placed within the originally two-component steady composite vortex structure has an area close to that of the inner vortex, then the resulting steady three-component vortex will differ in its characteristics

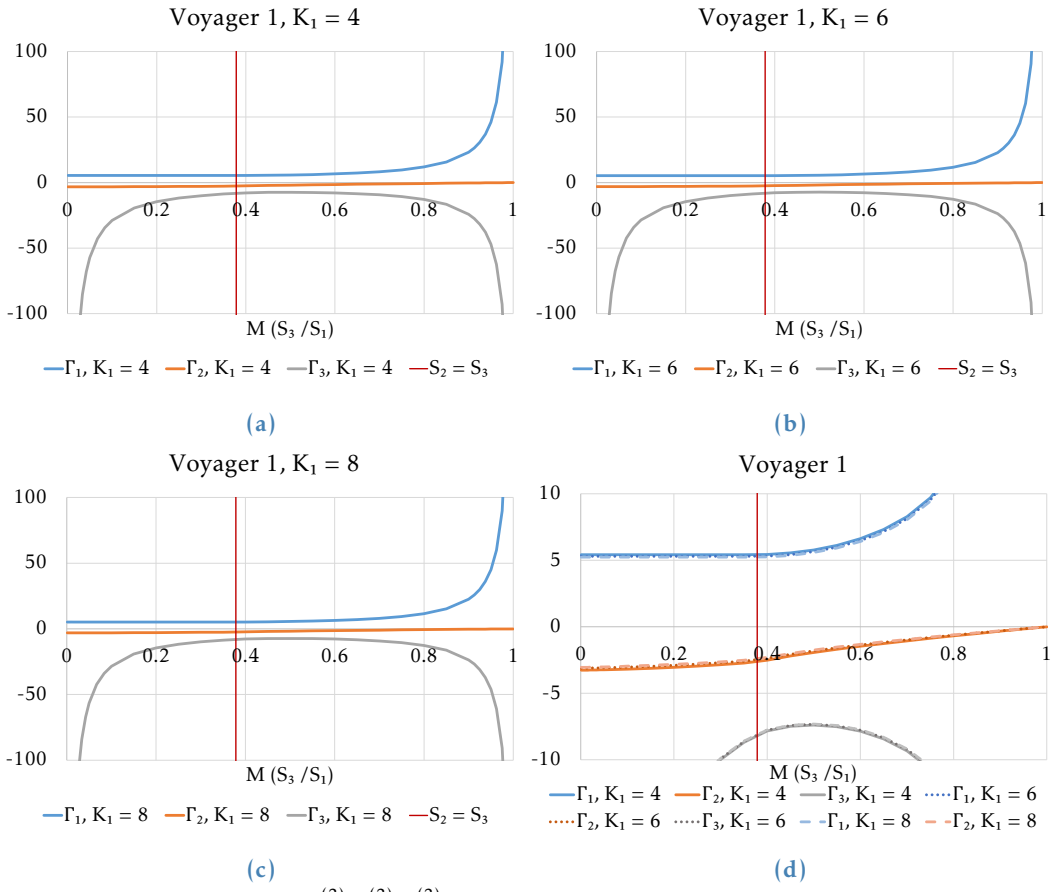


Figure 2. Intrinsic vortices $(\Gamma_1^{(3)}, \Gamma_2^{(3)}, \Gamma_3^{(3)})$ as a function of the size of the third vortex (parameter $M = \frac{a_3 b_3}{a_1 b_1}$) for (a) $K_1 = 4$, (b) $K_1 = 6$, (c) $K_1 = 8$ for the Voyager 1 mission. The vertical red line indicates the coincidence of vortices #2 and #3, $S_2 = S_3$. Panel (d) repeats panel (b) with a more detailed scale on the y-axis and for all values of K_1.

from the original two-component vortex by practically nothing, except for a very narrow zone between the two inner vortices. The potential vorticity in this narrow zone turns out to be finite, and in the limit where the areas of the specified vortices coincide, this zone will disappear, and the three-component and two-component vortices will become equivalent. In other words, adding a third vortex–one similar in size to the inner vortex–to a system of two vortices will not lead to a significant change in the characteristics of the new three-component system. That is, in this case, the structural stability of a stationary composite vortex is observed. There is reason to believe that this property of structural stability will also hold true for composite vortices with an arbitrary number of embedded vortices. This, in turn, indirectly suggests that it is possible to construct a composite vortex with a continuous distribution of potential vorticity in the inner zone.

Figure 3d illustrates the fact that the properties of two-component and three-component composite vortices coincide, provided that $S_2 = S_3$. Here, on a more convenient scale along the y-axis, the dependence of the total potential vorticity of all zones in a three-component composite vortex system on M is shown. The red vertical line corresponds to the condition $S_2 = S_3$. The crosses on the curves $(1 + \Gamma_1^{(3)} + \Gamma_2^{(3)} + \Gamma_3^{(3)})$ and $(1 + \Gamma_1^{(3)})$ correspond to the numerical values $(1 + \Gamma_1^{(2)} + \Gamma_2^{(2)})$ and $(1 + \Gamma_1^{(2)})$, respectively, for a two-component vortex when $S_2 = S_3$ and demonstrate that the conditions are satisfied for a specific value of the parameter M:

$$\begin{cases} (1 + \Gamma_1^{(3)} + \Gamma_2^{(3)} + \Gamma_3^{(3)}) = (1 + \Gamma_1^{(2)} + \Gamma_2^{(2)}) \\ (1 + \Gamma_1^{(3)}) = (1 + \Gamma_1^{(2)}) \end{cases}. \tag{30}$$

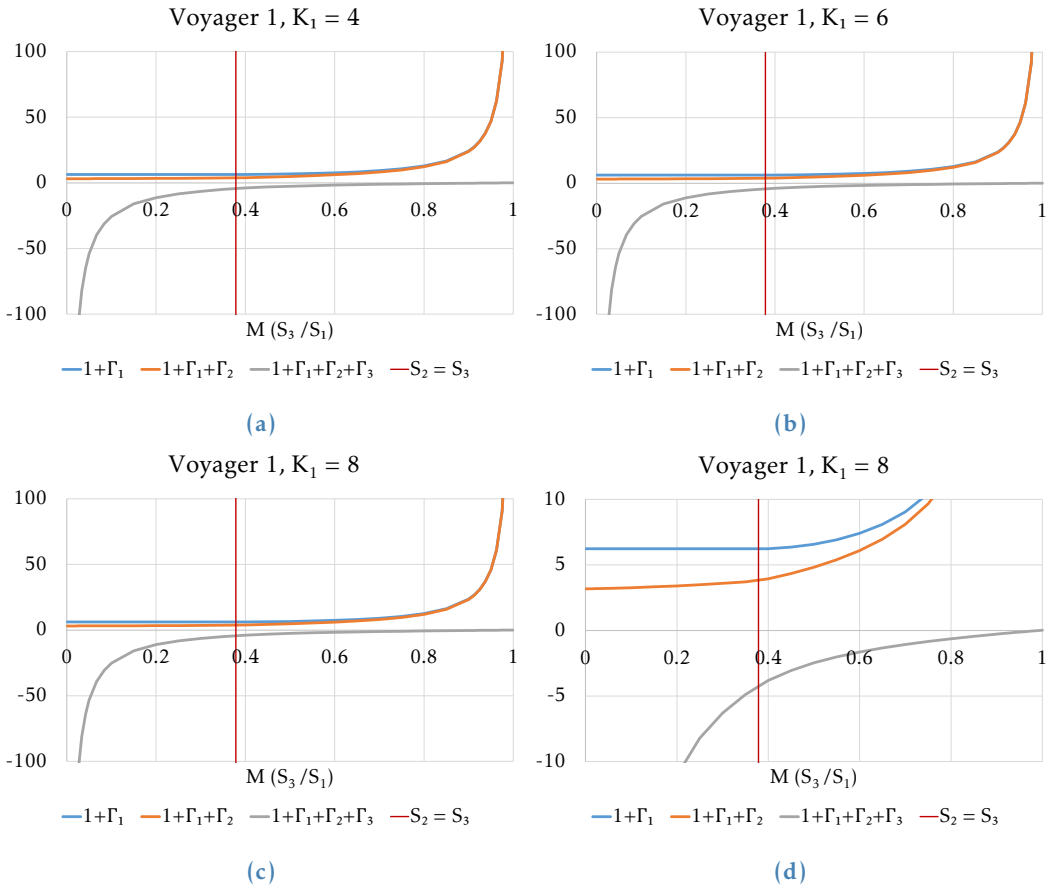


Figure 3. Total vorticity of various zones of a three-component composite vortex $(1+\Gamma_1^{(3)})$, $(1+\Gamma_1^{(3)}+\Gamma_2^{(3)})$, $(1+\Gamma_1^{(3)}+\Gamma_2^{(3)}+\Gamma_3^{(3)})$ as a function of the size of the third vortex (parameter $M=\frac{a_3b_3}{a_1b_1}$) for three values of $K_1=4,6,8$ for the Voyager 1 mission. The vertical red line indicates the coincidence of vortices #2 and #3, $S_2=S_3$. The crosses denote the values $(1+\Gamma_1^{(2)})$ and $(1+\Gamma_1^{(2)}+\Gamma_2^{(2)})$ for the condition $S_2=S_3$.

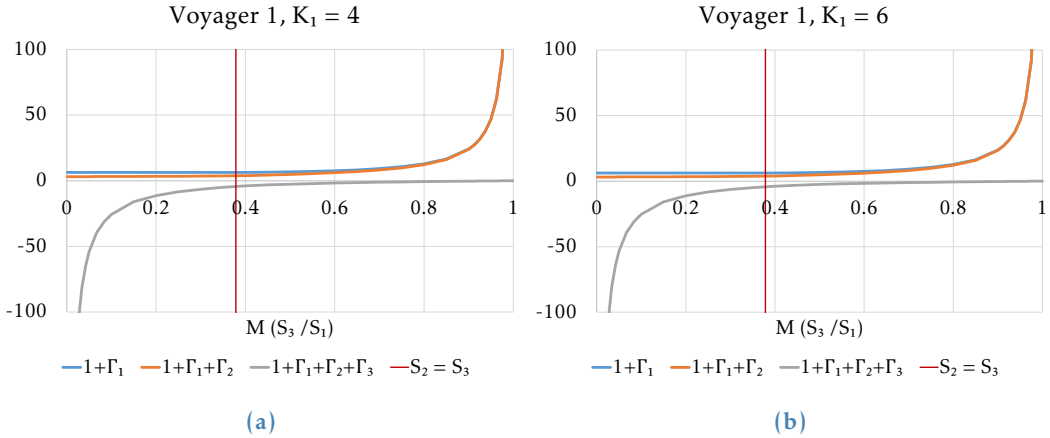


Figure 4. Average potential vorticity of the GRS over volume $\langle\Gamma\rangle_V$ (a) and over area $\langle\Gamma\rangle_S$ (b) of the main cross-section for three values of $K_1=4,6,8$ for the Voyager 1 mission as a function of the size of the third vortex (parameter $M=\frac{a_3b_3}{a_1b_1}$). The vertical red line indicates the coincidence of vortices #2 and #3, $S_2=S_3$.

The specified conditions (30) hold for all missions and all values of K_1 used.

Ultimately, the potential vorticity of all the specified zones–averaged over the volume of the entire vortex or averaged over the area of all the specified zones on the main

horizontal cross-section of the vortex–exhibits an interesting property. It turned out that the volume-averaged values do not depend on the size of the third embedded vortex, but depend slightly on the vertical size of the main vortex, via the parameter K_1. This dependence is shown in Figures 4a and 4b for the Voyager 1 mission. Average values of $\langle\Gamma\rangle_V$ and $\langle\Gamma\rangle_S$ and their dependence on the size of the third vortex were calculated for all missions. It appears that in the range of values $4 \le K_1 \le 8$, the average volume-averaged potential vorticities of the entire vortex differ from one another by less than 10 %. Therefore, it can be concluded that the dependence of the average values on the vertical size of the vortex can also be neglected. As results, the volume-averaged potential vorticity of the vortex $\langle\sigma\rangle_V$, in dimensional form, is related exclusively to the background flow shear Γ and is linearly dependent on it. As the estimates reveal, $\langle\sigma\rangle_S$ depends both on the sizes of the embedded vortices that make up the composite vortex structure and on the vertical size K_1 of the main vortex. However, the variations in $\langle\sigma\rangle_S$ associated with both the size of the vortices and the value of K_1 are even smaller than the variations in $\langle\sigma\rangle_V$. Therefore, both $\langle\sigma\rangle_V$ and $\langle\sigma\rangle_S$ can be considered identical with acceptable accuracy for the conditions in each mission. They are both linearly related to the shear parameter Γ: $\langle\sigma\rangle_V = \langle\sigma\rangle_S = k\Gamma$, where k is the proportionality coefficient. However, the proportionality coefficient varies significantly from mission to mission. Thus, according to our estimates, for the Voyager 1 mission in 1979, $k \approx 1.3 \div 1.4$; for Galileo in 1996, $k \approx 1.7 \div 1.9$; for Cassini in 2000, $k \approx 2.8 \div 3.1$; and for the HST (Hubble Space Telescope), in 2006, $k \approx 2.9 \div 3.1$. That is, for some reason, the proportionality coefficient increases over time and is not a universal constant. At the same time, the shear of the background flow Γ decreases over time, which somewhat stabilizes the changes in the product $k\Gamma$.

Thus, an examination of the structural stability of a two-component stationary composite vortex–by creating a three-component stationary vortex structure from it–revealed the following. If the third vortex differs significantly in cross-sectional area from the other two vortices, then the quantitative characteristics of the resulting three-component vortex differ greatly from those of its counterparts in the two-component vortex. If, however, the third vortex practically coincides with the inner vortex of the considered system of embedded vortices, then the characteristics of the three-component vortex system differ almost not at all from those of the two-component vortex. We interpret the obtained properties as the possibility of a smooth transition from a three-component vortex to a two-component vortex.

In the general case, the numerical values of all parameters of a two-component composite vortex structure change significantly when a third vortex is introduced into it. However, the overall qualitative properties of the two vortex configurations remain unchanged. In particular, the characteristics of the vortex system for the limiting sizes of the embedded vortices are preserved as $M \to 0$ and $M \to 1$. The smallest inner vortex will necessarily have the opposite sign of particle rotation compared to the rotation of particles in the outer shell. The largest vortex always remains anticyclonic. The medium-sized embedded vortex, while remaining anticyclonic, occupies an intermediate position in terms of vorticity within the hierarchy of the three vortices. However, if the third vortex is similar in size to the inner vortex of a two-component structure, then such a three-component composite vortex turns out to be closer in its characteristics to a two-component vortex. When the two inner vortices coincide completely, the three-component vortex degenerates into a two-component vortex system with complete coincidence of the vorticity of all its constituent parts. In other words, a three-component vortex smoothly transforms into a two-component vortex structure, along with its physical characteristics. This property proves that a two-component vortex is structurally stable with respect to perturbation by its third embedded vortex.

A similar question has previously been formulated for single-component homogeneous vortices and two-component vortices. What limiting vortex system results from a two-component stationary vortex if the volume of the embedded inner vortex is made to approach zero? This problem was studied in [*Arakelyan et al.*, 2026a]. It appears that

the limiting two-component vortex with zero volume of the embedded inner vortex is qualitatively different from a homogeneous one-component vortex [*Suetin et al.*, 2023]. This implies that there is no smooth transition between these two types of vortices, and in this sense, a homogeneous single-component vortex is structurally unstable with respect to perturbation by its embedded vortex.

The formal reason for the structural stability of the aforementioned vortices, in the general case, is the stationarity condition of the entire vortex system. Under conditions of stationarity at all boundaries within a composite vortex, it is not possible to perturb such a vortex system with a weak additional vortex and still expect the system to remain stationary. The potential vorticity of the perturbing vortex can be uniquely determined from the stationarity conditions of the vortex system. However, if we assume that the boundary of the perturbing vortex is not stationary and consider the perturbing vortex to be weak, then such a vortex will not affect the behavior of the boundaries of the other vortices. The initial composite vortex will remain stationary. In this physical formulation, the composite vortex will remain a stable vortex structure. The task of describing the perturbed vortex system reduces to describing the behavior of the perturbing vortex in the flow field of the initial composite vortex.

A similar problem, in which a stationary, homogeneous (in terms of potential vorticity) ellipsoidal vortex was considered as the initial vortex system, and a weak, smaller vortex placed inside the initial vortex, was studied in [*Arakelyan et al.*, 2026b]. Let us label the perturbing vortex the probe vortex. The behavior of the probe vortex turned out to be as follows. If the centers of both vortices do not coincide at the initial moment, then the probe vortex as a whole will move along a closed elliptical orbit; its shape will rotate simultaneously with the motion and undergo limited deformation, remaining ellipsoidal. If, however, the centers of the vortices coincide at the initial moment, then such a vortex as a whole will not move; however, it may rotate and undergo limited deformation. Details of the description can be found in the cited work.

Let us consider a closely related problem here. As the initial vortex system, we will take the two-component composite vortex discussed in [*Arakelyan et al.*, 2026a], or the three-component stationary vortex proposed in this study. As a probe vortex, we will take a weak ellipsoidal vortex completely embedded in the central zone of the initial vortex (let us call this zone the eye of the vortex system) or in the gap between the boundaries of the embedded vortices.

Centers of the probe vortex and the main vortex do not necessarily have to coincide, but the boundaries of the inner vortex of the composite system and the probe vortex must not touch at any point. This problem is equivalent to the behavior of the probe vortex in an isovortex background flow created by embedded vortices in their common central zone. Since the specified eye region is located within several vortex cores of the composite vortex at once, the total field of the isovorticity flow from all vortices is linear in the coordinates and exhibits well-defined properties when acting on the probe vortex. This problem is described below in the Appendix, where the following properties of the moving probe vortex are derived. In particular, the probe vortex will move along a closed ellipsoidal trajectory at the velocity of the composite vortex flow at its center. If the centers of the probe vortex and the initial composite vortex coincide, then the probe vortex as a whole will remain stationary, but its boundary will evolve. The behavior of the boundary, however, is not dependent on whether the probe vortex moves or remains stationary. Everything is determined by the relationship between two properties of this background flow: the tendency to stretch the probe vortex due to the inhomogeneity of the background flow itself, and the ability to rotate the vortex, taking into account the effects of the probe vortex's own rotation.

If the rotational properties are more pronounced than the stretching properties, then in such a flow the vortex cannot stretch into a filament. It will remain a spatially localized structure capable only of rotating or undergoing nutational oscillations with limited changes in the size of the vortex core. It is precisely this situation that occurs inside

a steady-state single-component vortex [*Arakelyan et al.*, 2026b]. As for the behavior of probe vortices in more complex composite vortices placed in any region of these stationary vortex structures, they all possess an important property: their energy cannot increase indefinitely. The energy behavior of probe vortices is periodic if they remain spatially localized formations (in a state of rotation or nutation). If the energy is small at the initial moment, it will remain small. If, however, the probe vortices stretch into vortex filaments, their intrinsic energy will eventually tend toward zero. In any case, test vortices cannot significantly affect the entire vortex system, which, under this type of perturbation, will remain a stable vortex structure. A perturbation of a composite vortex in the form of a probe vortex does not lead to the instability of the composite vortex.

4. Discussion of the Results and Future Perspectives

This paper investigates and reinterprets the properties of baroclinic mesoscale vortices in a background flow, representing models of Jupiter's Great Red Spot obtained in [*Arakelyan et al.*, 2026a,b; *Suetin et al.*, 2023]. The simplest model is a stationary ellipsoidal vortex with uniform, constant core vorticity in a horizontal shear flow [*Suetin et al.*, 2023]. Next, we consider a two-component vortex consisting of two nested stationary ellipsoidal, confocal vortices under the influence of the same background flow [*Arakelyan et al.*, 2026a]. Finally, we explore the stability of a homogeneous vortex in the presence of a perturbation in the form of a weak, nonstationary ellipsoidal vortex evolving within the vortex core. As a result, a very unusual property was discovered for a two-component steady vortex: an attempt to form a homogeneous vortex from it by reducing the volume of the inner vortex to zero revealed a new property. The resulting limiting vortex did not coincide with the homogeneous vortex previously studied in [*Suetin et al.*, 2023] in terms of either quantitative or qualitative characteristics. Inside such a vortex, a singularity formed in the form of a δ-function distributed over the volume of an infinitesimally small, confocal ellipsoid that had collapsed into an ellipse located in the vertical plane along the major horizontal axis of the main vortex. The integral volumetric vorticity of this feature accounted for more than 30 % of the integral vorticity of the main vortex. The calculations were performed under GRS conditions. We interpreted this fact as a structural instability of the two-component vortex. Due to the arising feature, the structure of its core differs qualitatively from that of a homogeneous vortex. This property raised a new question: what properties would a three-component vortex have? (1) Would it exhibit a similar feature if the volume of the smallest vortex were reduced to zero? (2) What will happen if the two inner vortices merge? Would a new δ-shaped singularity arise in the gap between the boundaries of the adjacent inner vortices? If so, how should it be interpreted? If the answer to the first question is "yes" and the answer to the second is "no," the three-component vortex will remain structurally stable relative to a two-component composite vortex. That is, no qualitatively new properties will be observed in it. In all other cases, the three-component vortex will prove to be structurally unstable relative to the two-component vortex. Then, new qualitative properties will appear in its core, and its structure will undergo a qualitative reorganization.

Based on an analysis of the results, our study yields the following conclusions. The three-component vortex appears to be structurally stable. That is, when the volume of the smallest vortex is reduced to zero, a singularity does indeed arise within it, analogous to the singularity of a two-component vortex. When the boundaries of the two inner vortices converge, no singularities arise. When the geometric dimensions are changed, all parameters of the three-component vortex vary continuously. When the dimensions of the two inner vortices coincide, the vorticity distribution of the core of the three-component vortex coincides with the corresponding distribution of the two-component vortex.

In turn, this result leads to new questions. Will new qualitative properties emerge if the structure of the composite vortex is made more complex? For example, by studying a multi-component composite vortex consisting of four, five, and so on, nested vortices. In the case of structural stability of a multi-component composite vortex, it is possible–by

tightly packing the inner vortices–to limit the model to one with a continuous distribution of the core's potential vorticity. This is a separate problem that remains to be addressed. However, it is precisely the three-component model that suggests that a multi-component composite vortex is also structurally stable. It can be predicted in advance that in such a continuous model, the concept of the "eye of the vortex" will need to be introduced. This is the central part of the vortex, an ellipsoidal shape of finite size with uniform vorticity. If the volume of this zone is reduced to zero, a δ-shaped singularity similar to the one described above will arise. The "eye of the vortex" is needed to avoid this. Outside the eye of the vortex, there will be a zone with a smooth distribution of potential vorticity.

The three-component model replicated a number of properties of the two-component model. Both variants were based on GRS conditions in the calculations. In particular, in the central part of the vortex, both model variants predict relatively weak cyclonic particle motion. In the peripheral zone, a strong anticyclonic flow emerged. It is precisely this property that is observed in reality. It is interesting to note that in the three-component model, the vortex of intermediate size also caused the rotation of particles in an anticyclonic direction. Why? First and foremost, we must take into account that all geometric properties, as well as the background velocity shear and other necessary characteristics, were derived from observations. The resulting properties are specific to the GRS. If we change the geometry of the vortices or other parameters, this same model may exhibit different properties. In our model, we can explain why the intermediate vortex also rotates the particles in an anticyclonic direction, just like the peripheral jet. Note that two- and three-component models are a certain approximation (perhaps a rough one) of a model with a continuous distribution of potential vorticity. Therefore, one would expect that in the transition zone from weak cyclonic motion in the central region to intense anticyclonic motion at the periphery, the influence of the strong anticyclonic component would be more significant. Consequently, one would expect predominantly anticyclonic motion in this region as well. The three-component model, in fact, demonstrates exactly that.

Let us discuss the problem presented in the Appendix. Essentially, this problem addresses the stability of a multicomponent composite vortex against a disturbance in the form of a small, weak vortex. Such a vortex is referred to here as a probe vortex. The proposed problem is not a comprehensive stability analysis, but rather a problem concerning stability against a specific type of perturbation. The test vortex moves and deforms due to both the flow of the multicomponent vortex itself and the background shear flow. The probe vortex can gain or lose energy from flows external to it. This problem generalizes the work in [*Arakelyan et al.*, 2026b], where the probe vortex evolves within a vortex structure that is homogeneous in terms of vorticity [*Arakelyan et al.*, 2026a], modeling a two-component composite vortex consisting of a non-stationary inner part (the probe vortex) and a stationary outer part (the main vortex). In [*Arakelyan et al.*, 2026b], the problem of the motion of the probe vortex as a whole is solved, and this solution is supplemented by a description of the deformation of the vortex's shape and its rotation. It is shown that such a vortex exchanges energy quasi-periodically with the flow external to it and, being weak at the initial moment, will remain weak thereafter. The problem of a non-stationary internal vortex arose due to a purely mathematical property of stationary multicomponent vortices: the potential vorticity of the entire set of vortices comprising a composite vortex is uniquely determined by the shift of the background flow and the geometry of the embedded vortices. It is impossible to embed another vortex with arbitrary potential vorticity into a stationary vortex. This is discussed in detail in this paper for two- and three-component vortices and remains true for multicomponent stationary vortices. Very strict conditions are imposed on the creation of stationary composite vortices. An arbitrary embedded vortex, on the other hand, will necessarily turn out to be non-stationary. This is precisely why the problem of a composite vortex with a non-stationary core arose.

As shown in the Appendix, the behavior of the probe vortex in the central part of a complex composite vortex does not differ qualitatively from its behavior in a simple homogeneous vortex. The key property is that the probe vortex does not lead to instability

of the entire vortex system. Being energetically weak at the initial moment, it will remain weak thereafter. Moreover, its horizontal dimensions will vary in a limited, quasi-periodic manner. Such a vortex will remain a localized feature. In general, such a vortex should be included among the vortices that make up a composite vortex. In this case, the main large vortex will have a stationary (quasi-stationary) boundary, while the embedded vortex will constitute a non-stationary core.

Let us place a probe vortex in the gap between the stationary boundaries of the internal vortices of a composite vortex system. In this case, in addition to the localized evolution scenario already described, the probe vortex may exhibit another possible behavior. Specifically, the probe vortex may stretch into a vortex filament and, while remaining in the same region between the vortex boundaries, wind itself around the inner part of the composite vortex structure. In this case, the vortex's intrinsic energy will tend toward zero. The scenario according to which the probe vortex evolves depends on the external and initial conditions. However, this new behavior of the probe vortex does not lead to instability in the main vortex.

Finally, let us discuss the question of which model–stationary or non-stationary–the authors consider more physically plausible and better describes the reality of the GRS. That is, the choice is between a two- or three-component composite vortex (possibly with a continuous distribution of the core's potential vorticity) and a vortex with a time-varying core and a quasi-stationary outer part. We tend to believe that the non-stationary model is more realistic. Our arguments in favor of the non-stationary model are based on the following considerations. First, the stationary model requires, depending on the geometric dimensions of its components, quite specific and definite values for the potential vorticities of all vortices comprising the composite vortex. Any deviation in vorticities or dimensions will lead to non-stationarity. Second, over the course of 350 years of observations, a real vortex–albeit slowly–evolves over time in terms of its size, vorticity, and background flow parameters. And in any case, this vortex originated at some point in the past. For a vortex to emerge abruptly or rapidly reach a quasi-steady state, its parameters must be close to the specified values. But nature is unlikely to know that these parameters are specified and must be adhered to. Most likely, the vortex arose as a result of shear instability and is sustained by it. The rules governing the development of this instability are not tied to the conditions for vortex stationarity. Accordingly, one should not expect that the vorticity distribution resulting from the development of the instability will be sufficient to ensure the stationarity of the quantity. Third, in our model of a composite steady vortex, we use nested ellipsoids that are confocal with the main vortex and possess the following property: as their volume decreases, their horizontal elongation (the ratio of the major horizontal axis to the minor one) increases indefinitely. However, it is known that elongated ellipsoidal vortices are unstable and break up into a series of smaller but more circular vortices. For plane hydrodynamics, the critical ratio of the semi-axes is equal to three. In the three-dimensional case, this condition is violated, but not to a great extent. Therefore, in the central part of the vortex, one should expect the manifestation of instability and the appearance of smaller, rounded vortex structures. At the same time, these vortices exhibit non-stationary behavior. This is precisely what is observed in nature. When processing field observations, it is necessary to perform area smoothing, which eliminates small vortices and leads to the appearance of a single, larger vortex in the averaged field. If the resulting averaged vortex turns out to be confocal with the main vortex, then the entire system may become stationary. However, the data presented do not support confocality but rather correspond to similarity conditions with a ratio of horizontal semi-axes ranging from 1.6 to 2.2. Moreover, in every mission (Voyager 1 and 2 (1979), Galileo (2009), Cassini (1995–2003), and observations from the Hubble Space Telescope), the main and inner vortices were considered similar, but the similarity coefficients varied from mission to mission. The similarity condition, however, suggests that the embedded vortex is non-stationary.

Thus, the authors tend to believe that a nonstationary model is better suited to describing the actual GRS. However, there is still no complete clarity on this issue.

5. Conclusions

We have solved the problem of a stationary composite vortex consisting of three embedded, ellipsoidal, confocal vortex structures in the quasi-geostrophic approximation in a rotating, density-stratified atmosphere on the f-plane. The proposed solution is an exact solution to the nonlinear equation of conservation of potential vorticity in the quasi-geostrophic approximation, taking into account nonlinear boundary conditions on the surfaces of all three vortices. The obtained solution for the three-component vortex was compared with a similar solution for a two-component vortex considered earlier. The analysis revealed the following. If the sizes of the two vortices in a three-component vortex structure are fixed, and the behavior of the vortex characteristics is then studied as a function of the size of the third vortex, the quantitative physical properties of the two-component and three-component structures will differ significantly from one another, provided that the size of the third vortex differs significantly from the sizes of the other vortices. However, if the size of the third vortex is close to that of the inner vortex of the three-component system, then the physical parameters of the three-component vortex system approach those of a two-component vortex. When these sizes coincide exactly, the characteristics of the two- and three-component vortices also coincide. We interpret this fact as the structural stability of a two-vortex system against the perturbation of a third vortex, provided that the size of the perturbing vortex is close to that of the system's inner vortex. A similar problem concerning the structural stability of a homogeneous vortex system against the perturbation of a second vortex in a steady-state setting is solved in favor of the structural instability of such a composite vortex system. There is no continuous transition of the physical properties of a two-component composite vortex structure to the characteristics of a single-component homogeneous vortex as the volume of the internal vortex is reduced to zero.

The properties mentioned above were obtained under the assumption that all boundaries in the vortex system are stationary. Removing the stationarity assumption allows us to examine the evolution of a small, weak disturbance vortex (referred to in this paper as a probe vortex) in the flow field of a vortex system, provided that the probe vortex does not affect the behavior of the boundaries of the multicomponent vortex. In this case, depending on its initial position and physical characteristics, the non-stationary probe vortex may remain limited in size or stretch into a vortex filament, moving as a whole along a closed elliptical trajectory. If, however, the center of the probe vortex coincides with the center of the composite vortex, then the probe vortex as a whole will remain stationary, but its boundary will evolve. In either case, the energy of the probe vortex will remain finite. Consequently, small, weak vortices placed inside a multicomponent vortex cannot lead to the instability of the composite vortex system in question.

Acknowledgments. The authors express their gratitude to the anonymous reviewers for their constructive comments.

Funding. This work was supported by the P. P. Shirshov Institute of Oceanology, Russian Academy of Sciences [State Assignment No. FMWE-2024-0016] (problem formulation, theoretical part of the work), the A.M. Obukhov Institute of Atmospheric Physics, Russian Academy of Sciences [State Assignment No. FMWR-2025-0009] (analysis of results), Peter the Great St. Petersburg Polytechnic University [Grant No. FSEG-2026-0020] (development of the application), and the Russian Science Foundation [Grant No. 25-17-00021] (computational part of the work).

Appendix A. The Dynamics of a Weak, Small, Non-Stationary Vortex within the Core of a Large, Stationary, Multicomponent Vortex Structure

It was shown above that, in the case of a composite vortex consisting of two stationary vortices embedded within one another, each vortex influences the behavior of the boundary of the other vortex. The conditions of stationarity and confocality imply that the parameters

of both vortices are rigidly coupled to one another and to the value of the background velocity shear Γ. At the same time, it is clear from physical considerations that if the size of the inner vortex is small compared to the size of the larger vortex and its integral potential vorticity (the intensity of the inner vortex) is weak in comparison to the main vortex, then the inner vortex does not affect the behavior of the boundary of the larger vortex. In this case, the large vortex and the background flow merely act on the small vortex, deforming its boundary, while the influence of the small vortex has virtually no effect on the behavior of the large vortex's boundary. In this case, the boundary of the main vortex can still be considered stationary and independent of the small vortex. The behavior of the small vortex, on the other hand, can be viewed as its evolution in the flow field of the large vortex and the general background flow with a shear. In this case, the rigid connection between the intensities of the two vortices disappears. It then becomes possible to consider the small vortex as a non-stationary vortex with arbitrary intensity.

This can be called a "probe", analogous to a probe charge in the study of electromagnetic fields. A probe vortex is a small, weak vortex placed inside a large vortex that does not affect the boundary of the large vortex and is not bound to the large vortex by the condition of stationarity of its boundary. This part of the study can be viewed as a relatively independent investigation into the behavior of a small test vortex inside the core of a large vortex. The background flow for the test vortex is a superposition of the flow from the large vortex within its core and the background horizontal barotropic flow with a shear, within which the entire vortex structure is embedded. Both of these flows are linear in the horizontal coordinates. Consequently, if the inner vortex has an ellipsoidal core shape at the initial time, it will remain an ellipsoidal vortex thereafter. This allows us to apply the theory of ellipsoidal vortex behavior against a background of barotropic, equally vortex flows.

This theory was originally presented in [*Zhmur and Pankratov*, 1989] and subsequently reproduced in the monograph [*Zhmur*, 2011]. It is described most rigorously and comprehensively in [*Zhmur et al.*, 2023]. According to the conclusions of this approach, an ellipsoidal vortex in an isovortical barotropic background flow moves as a whole at the velocity of the background flow at the vortex center. At the same time, its boundary (shape) may rotate, undergo nutational oscillations, or stretch indefinitely. There are only three types of behavior for the boundary of a vortex core. The evolutionary scenario for such a vortex depends on the dimensionless parameter $|\gamma/e|$ of the flow $\overrightarrow{u}_f$, external to the vortex, where $\gamma = \frac{1}{2}\mathrm{rot}_z \overrightarrow{u}_f$, and e is the deformation coefficient. When $|\gamma/e| > 1$, the modes of rotation and nutational oscillations are possible, and the mode of unrestricted elongation is impossible. In other words, when $|\gamma/e| > 1$, the vortex remains a localized structure throughout its evolution. When $|\gamma/e| < 1$, all three modes of vortex behavior are possible, including unrestricted vortex elongation. A more detailed description of these modes is available in [*Suetin et al.*, 2023].

First, we will discuss the modes of behavior of a small vortex.

The deformation component of an arbitrary background barotropic flow, which is linear in the horizontal coordinates, can be written as:

$$\begin{pmatrix} u_f \\ v_f \end{pmatrix} = \begin{pmatrix} e & -\gamma_1 \\ \gamma_2 & -e \end{pmatrix} \begin{pmatrix} x \\ y \end{pmatrix}. \tag{A1}$$

In this type of flow, the evolution of the vortex parameters follows the following rules [*Zhmur*, 2011; *Zhmur and Pankratov*, 1989]:

$$\begin{cases} \dot{\varepsilon} = 2\varepsilon\left(e\cos 2\theta - \dfrac{1}{2}(\gamma_1 - \gamma_2)\sin 2\theta\right) \\ \dot{\theta} = \Omega(\varepsilon, K) + \dfrac{1}{2}(\gamma_1 + \gamma_2) - \dfrac{\varepsilon^2 + 1}{\varepsilon^2 - 1}\left(e\sin 2\theta + \dfrac{1}{2}(\gamma_1 - \gamma_2)\cos 2\theta\right) \end{cases}. \tag{A2}$$

Here, e, γ_1, and γ_2 are the background flow coefficients associated with a certain horizontal coordinate system (x, y). Moreover, $\gamma_1 + \gamma_2 = \mathrm{rot}_z \overrightarrow{u}_f$. The parameter $\varepsilon = \frac{a}{b}$ describes the horizontal elongation of the vortex core, and $K = \frac{\tilde{c}}{\sqrt{ab}}$ describes its vertical flattening. The angle θ is the orientation angle of the vortex core in the chosen (x, y) coordinate system (see Figure A1). The parameters a and b are the horizontal semi-axes of the ellipsoid; $\tilde{c} = \frac{N}{f}c$, where c is the vertical semi-axis. $\Omega(\varepsilon, K)$ is the natural angular velocity of rotation of the vortex core's shape. Details can be found in [*Zhmur and Pankratov*, 1989].

In another analogous coordinate system $\tilde{x}, \tilde{y}$, rotated by an angle α relative to (x, y), the background flow $(\tilde{u}, \tilde{v})$ remains linear in $\tilde{x}, \tilde{y}$, but with different coefficients $\tilde{e}, \tilde{\gamma}_1, \tilde{\gamma}_2$:

$$\begin{pmatrix} \tilde{u} \\ \tilde{v} \end{pmatrix} = \begin{pmatrix} \tilde{e} & -\tilde{\gamma}_1 \\ \tilde{\gamma}_2 & -\tilde{e} \end{pmatrix} \begin{pmatrix} \tilde{x} \\ \tilde{y} \end{pmatrix}. \tag{A3}$$

The behavior of the vortex core's characteristics will be described by equations identical to those in Equation (A2), in which the following obvious substitutions must be made: $e, \gamma_1, \gamma_2, \theta$ to $\tilde{e}, \tilde{\gamma}_1, \tilde{\gamma}_2, \tilde{\theta}$, respectively. In this case, the old parameters $e, \gamma_1, \gamma_2, \theta$ in (A2) and the new parameters $\tilde{e}, \tilde{\gamma}_1, \tilde{\gamma}_2, \tilde{\theta}$ in (A3) are related by the following equations:

$$\begin{aligned} \tilde{e} &= e\cos 2\alpha - \frac{1}{2}(\gamma_1 - \gamma_2)\sin 2\alpha, \\ \tilde{\gamma}_1 &= e\sin 2\alpha + \frac{1}{2}(\gamma_1 + \gamma_2) + \frac{1}{2}(\gamma_1 - \gamma_2)\cos 2\alpha, \\ \tilde{\gamma}_2 &= -e\sin 2\alpha + \frac{1}{2}(\gamma_1 + \gamma_2) - \frac{1}{2}(\gamma_1 - \gamma_2)\cos 2\alpha, \\ \tilde{\theta} &= \theta - \alpha. \end{aligned} \tag{A4}$$

Let us choose a coordinate system $\tilde{x}, \tilde{y}$ in which the coefficients $\tilde{\gamma}_1$ and $\tilde{\gamma}_2$ are equal: $\tilde{\gamma}_1 = \tilde{\gamma}_2$. In this coordinate system, the coefficient $\tilde{e}$ is the deformation coefficient. This coordinate system is useful for studying the behavior of vortices in background flows and was proposed by Kida [*Kida*, 1981] for these purposes in 2D hydrodynamics.

Consider a system of N confocal ellipsoidal vortices embedded within one another and elongated along the x-axis. For the sake of clarity, we will number the vortices, starting with the largest (numbered #1) and ending with the smallest (numbered #N). We will refer to the inner part of the smallest vortex, numbered #N, as the eye of the multipole vortex. The goal of this part of the study is to describe the flow within the eye of the vortex system and to investigate the behavior of a probe vortex in this area.

As the initial (x, y) coordinate system for geophysical applications, we will choose a convenient system in which the x-axis points east and the y-axis points north. In such a coordinate system, within the core of the main vortex, in its eye, there is a flow (u_f, v_f) that serves as the background for the probe vortex:

$$\begin{cases} u_f = -\left(\Gamma + \frac{1}{2}\sigma_1\beta_0^{(1)} + \frac{1}{2}\sigma_2\beta_0^{(2)} + \frac{1}{2}\sigma_3\beta_0^{(3)} + \ldots\right)y \\ v_f = \left(\frac{1}{2}\sigma_1\alpha_0^{(1)} + \frac{1}{2}\sigma_2\alpha_0^{(2)} + \frac{1}{2}\sigma_3\alpha_0^{(3)} + \ldots\right)x \end{cases}.$$

Here, the coefficients e, γ_1 and γ_2 are explicitly given:

$$\begin{aligned} e &= 0, \\ \gamma_1 &= \Gamma + \frac{1}{2}\sigma_1\beta_0^{(1)} + \frac{1}{2}\sigma_2\beta_0^{(2)} + \frac{1}{2}\sigma_3\beta_0^{(3)} + \ldots = \Gamma + \frac{1}{2}\sum_{i=1}^{N}\sigma_i\beta_0^{(i)}, \\ \gamma_2 &= \frac{1}{2}\sigma_1\alpha_0^{(1)} + \frac{1}{2}\sigma_2\alpha_0^{(2)} + \frac{1}{2}\sigma_3\alpha_0^{(3)} + \ldots = \frac{1}{2}\sum_{i=1}^{N}\sigma_i\alpha_0^{(i)}. \end{aligned}$$

The requirement that the vortex system be stationary leads to a unique determination of the intrinsic vortices σ_i. Therefore, the signs of γ_1 and γ_2 are well-defined for this coordinate system.

When rotated by an angle α, the coefficients (e, γ_1, γ_2) in Equation (A2) should be replaced by $\tilde{e}, \tilde{\gamma}_1, \tilde{\gamma}_2$, according to relations (A4). The equality condition $\tilde{\gamma}_1 = \tilde{\gamma}_2$ yields an equation for the rotation angle:

$$e\sin 2\alpha + \frac{1}{2}(\gamma_1+\gamma_2) + \frac{1}{2}(\gamma_1-\gamma_2)\cos 2\alpha = -e\sin 2\alpha + \frac{1}{2}(\gamma_1+\gamma_2) - \frac{1}{2}(\gamma_1-\gamma_2)\cos 2\alpha.$$

From which it follows that $\cos 2\alpha = 0$, $\sin 2\alpha = \pm 1$, $\alpha = \pm\frac{\pi}{4}$, and

$$\tilde{e} = e\cos 2\alpha - \frac{1}{2}(\gamma_1-\gamma_2)\sin 2\alpha = \mp\frac{1}{2}(\gamma_1-\gamma_2). \tag{A5}$$

For clarity, in Equation (A5) we will choose the "plus" sign, resulting in:

$$\tilde{e} = \frac{1}{2}\left(\Gamma + \frac{1}{2}\sum_{i=1}^{N}\sigma_i(\beta_0^{(i)} - \alpha_0^{(i)})\right),$$

$$\tilde{\gamma} = \tilde{\gamma}_1 = \tilde{\gamma}_2 = \frac{1}{2}\left(\Gamma + \frac{1}{2}\sum_{i=1}^{N}\sigma_i(\beta_0^{(i)} + \alpha_0^{(i)})\right).$$

The parameter we are looking for will take the form:

$$\left|\frac{\tilde{\gamma}}{\tilde{e}}\right| = \frac{\left|\Gamma + \frac{1}{2}\sum\limits_{i=1}^{N}\sigma_i(\beta_0^{(i)} + \alpha_0^{(i)})\right|}{\left|\Gamma + \frac{1}{2}\sum\limits_{i=1}^{N}\sigma_i(\beta_0^{(i)} - \alpha_0^{(i)})\right|}. \tag{A6}$$

Depending on whether the inequality $|\tilde{\gamma}/\tilde{e}| > 1$ holds or not, the behavior of the probe vortex differs. If $|\tilde{\gamma}/\tilde{e}| > 1$, then the horizontal semi-axes of the probe vortex will remain finite in size, and consequently, the probe vortex itself will remain a localized structure. When $|\tilde{\gamma}/\tilde{e}| < 1$, a regime of unbounded elongation is possible, in which case the test vortex itself may deform into a vortex filament in the plane. A complete mathematical study of the behavior of the probe vortex in a system of N confocal vortices embedded within one another has not yet been undertaken. However, in the simplest case of a single homogeneous vortex with $N = 1$, the condition $|\tilde{\gamma}/\tilde{e}| > 1$ is automatically satisfied [*Suetin et al.*, 2023]. For a stationary composite vortex with $N = 2$, similar studies [*Arakelyan et al.*, 2026b] demonstrate the validity of the same inequality $|\tilde{\gamma}/\tilde{e}| > 1$ in its central region. Consequently, in at least two cases, it can be shown that the inequality $|\tilde{\gamma}/\tilde{e}| > 1$ holds for the central region of the composite vortex. As for the general case with arbitrary N, as well as the regions between the boundaries of vortices in a composite vortex system, no such studies have been carried out, and we cannot determine whether the inequality $|\tilde{\gamma}/\tilde{e}| > 1$ holds.

However, regardless of whether the inequality in question is fair or unfair by a factor of $|\tilde{\gamma}/\tilde{e}|$ and given that in isovortex flows, an ellipsoidal vortex exhibits only three modes of behavior–the rotational mode, the nutation mode, and the mode of unrestricted core elongation–the following general conclusion can be drawn. In the first two modes, periodic changes in the vortex's dimensions and oscillations of its eigenenergy occur. In these modes, the vortex remains a localized structure with finite dimensions and energy. In the mode of unrestricted core elongation, the vortex transforms into a vortex filament in the plane, and its energy decreases to zero. Consequently, in all three modes, the energy of a test vortex placed in any region within a stationary composite vortex cannot increase indefinitely: it either oscillates or decreases.

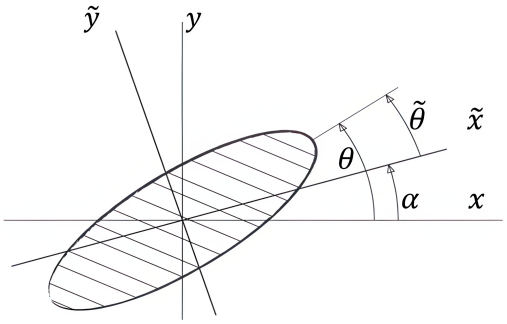


Figure A1. Position of the vortex in the old (x, y) coordinate system and the new $\tilde{x}, \tilde{y}$ coordinate system. Top view.

Appendix A.1. Trajectory of the Center of a Test Vortex

Let $x_0(t)$ and $y_0(t)$ denote the current coordinates of the center of a small vortex in the (x, y) coordinate system.

Since we assume that the center of the vortex moves with the background flow, taking into account the velocity field of that flow:

$$\begin{cases} u = -\left(\Gamma + \dfrac{1}{2}\displaystyle\sum_{i=1}^{N} \sigma_i \beta_0^{(i)}\right) y \\ v = \left(\dfrac{1}{2}\displaystyle\sum_{i=1}^{N} \sigma_i \alpha_0^{(i)}\right) x \end{cases}. \tag{A7}$$

We will derive the equations of motion for the vortex center:

$$\begin{cases} \dfrac{\mathrm{d}}{\mathrm{d}t} x_0(t) = -\left(\Gamma + \dfrac{1}{2}\displaystyle\sum_{i=1}^{N} \sigma_i \beta_0^{(i)}\right) y_0(t), \\ \dfrac{\mathrm{d}}{\mathrm{d}t} y_0(t) = \left(\dfrac{1}{2}\displaystyle\sum_{i=1}^{N} \sigma_i \alpha_0^{(i)}\right) x_0(t). \end{cases} \tag{A8}$$

The system (A8) can be reduced to a single equation for $x_0(t)$:

$$\frac{\mathrm{d}^2}{\mathrm{d}t^2} x_0(t) + \left(\Gamma + \frac{1}{2}\sum_{i=1}^{N} \sigma_i \beta_0^{(i)}\right)\left(\frac{1}{2}\sum_{i=1}^{N} \sigma_i \alpha_0^{(i)}\right) x_0(t) = 0. \tag{A9}$$

At the same time, there is a conservation integral in the system (A8):

$$\frac{\mathrm{d}}{\mathrm{d}t}\left\{ \frac{x_0^2(t)}{\left(\Gamma + \frac{1}{2}\sum\limits_{i=1}^{N} \sigma_i \beta_0^{(i)}\right)} + \frac{y_0^2(t)}{\frac{1}{2}\sum\limits_{i=1}^{N} \sigma_i \alpha_0^{(i)}} \right\} = 0. \tag{A10}$$

$$\frac{x_0^2(t)}{\left(\Gamma + \frac{1}{2}\sum\limits_{i=1}^{N} \sigma_i \beta_0^{(i)}\right)} + \frac{y_0^2(t)}{\frac{1}{2}\sum\limits_{i=1}^{N} \sigma_i \alpha_0^{(i)}} = \text{const}. \tag{A11}$$

Equation (A11) describes the general form of the motion trajectories, where "const" is determined by the initial conditions. Note that the intrinsic vortices σ_i satisfy a linear system of equations and must be determined at this stage. Consequently, the signs of the expressions $\Gamma + \frac{1}{2}\sum_{i=1}^{N} \sigma_i \beta_0^{(i)}$ and $\frac{1}{2}\sum_{i=1}^{N} \sigma_i \alpha_0^{(i)}$ in the denominator of Equation (A11) are

also determined. Equation (A11) generally describes elliptic or hyperbolic trajectories. However, hyperbolic trajectories are impossible for physical reasons–the trajectory cannot intersect with the inner boundaries of a multipole vortex, and the test vortex itself cannot leave the inner region of the vortex–its eye. Consequently, a situation arises in which the signs of $\left(\Gamma + \frac{1}{2}\sum_{i=1}^{N}\sigma_i\beta_0^{(i)}\right)$ and $\frac{1}{2}\sum_{i=1}^{N}\sigma_i\alpha_0^{(i)}$ are identical, and Equation (A11) describes an elliptical trajectory of motion that is entirely contained within the eye region of the vortex structure. As a result, the test vortex inside the eye of the composite vortex moves as a whole along an elliptical trajectory. According to Equation (A9), this motion is periodic with a frequency independent of the specific trajectory of motion:

$$\Omega = \sqrt{\left(\Gamma + \frac{1}{2}\sum_{i=1}^{N}\sigma_i\beta_0^{(i)}\right)\left(\frac{1}{2}\sum_{i=1}^{N}\sigma_i\alpha_0^{(i)}\right)}. \tag{A12}$$

In other words, all the small vortices moving as a whole within a large vortex complete one full rotation in the same amount of time.

Appendix A.2. Deformation of the Boundary of the Probe Vortex

Simultaneously with its overall motion, the shape of the core of the probe vortex undergoes periodic, limited deformations–rotation or nutational oscillations of the shape around a vertical axis–depending on the initial conditions for the vortex parameters.

If, at the initial moment, the center of the small vortex coincides with the center of the stationary large vortex, then the center of the small vortex does not move thereafter and remains at rest. However, its boundary (shape) will rotate or undergo nutational oscillations similar to the evolution of vortex shapes rotating around the center of the large vortex.

Equation (A12) allows us to introduce the characteristic time of the internal dynamics of the GRS–the period of rotation of the test vortex as a whole around the center of the composite vortex:

$$T = \frac{2\pi}{\Omega}.$$

If we take the simplified homogeneous GRS model [*Suetin et al.*, 2023] as the basic vortex, then the time T will be on the order of one Earth week.

References

Arakelyan E. M., Zhmur V. V. and Chkhetiani O. G. Composite Structure of Jupiter's Great Red Spot. Part 1. Stationary Model // Izvestiya, Atmospheric and Oceanic Physics. — 2026a. — Vol. 62, no. 3. — P. 403–424. — https://doi.org/10.1134/s0001433826700532

Arakelyan E. M., Zhmur V. V. and Chkhetiani O. G. Composite structure of Jupiter's Great Red Spot. Part 2. The non-stationary model // Izvestiya, Atmospheric and Oceanic Physics. — 2026b. — Vol. 62, no. 4. — P. 549–565. — https://doi.org/10.1134/S0001433826700933 — (In print).

Asay-Davis X. S., Marcus P. S., Wong M. H., et al. Jupiter's shrinking Great Red Spot and steady Oval BA: Velocity measurements with the 'Advection Corrected Correlation Image Velocimetry' automated cloud-tracking method // Icarus. — 2009. — Vol. 203, no. 1. — P. 164–188. — https://doi.org/10.1016/j.icarus.2009.05.001

Beaumont D. N. Solitary waves on an unsymmetrical shear flow with applications to Jupiter's Great Red Spot // Icarus. — 1980. — Vol. 41, no. 3. — P. 400–409. — https://doi.org/10.1016/0019-1035(80)90224-9

Bolton S. J., Levin S. M., Guillot T., et al. Microwave observations reveal the deep extent and structure of Jupiter's atmospheric vortices // Science. — 2021. — Vol. 374, no. 6570. — P. 968–972. — https://doi.org/10.1126/science.abf1015

Bouchet F. and Sommeria J. Emergence of intense jets and Jupiter's Great Red Spot as maximum-entropy structures // Journal of Fluid Mechanics. — 2002. — Vol. 464. — P. 165–207. — https://doi.org/10.1017/s0022112002008789

Choi D. S., Banfield D., Gierasch P., et al. Velocity and vorticity measurements of Jupiter's Great Red Spot using automated cloud feature tracking // Icarus. — 2007. — Vol. 188, no. 1. — P. 35–46. — https://doi.org/10.1016/j.icarus.2006.10.037

Dowling T. E. and Ingersoll A. P. Jupiter's Great Red Spot as a shallow water system // Journal of the Atmospheric Sciences. — 1989. — Vol. 46, no. 21. — P. 3256–3278. — https://doi.org/10.1175/1520-0469(1989)046<3256:jgrsaa>2.0.co;2

Flierl G. R. Baroclinic solitary waves with radial symmetry // Dynamics of Atmospheres and Oceans. — 1979. — Vol. 3, no. 1. — P. 15–38. — https://doi.org/10.1016/0377-0265(79)90034-4

Flierl G. R., Morrison P. J. and Vilasur Swaminathan R. Jovian vortices and jets // Fluids. — 2019. — Vol. 4, no. 2. — P. 104. — https://doi.org/10.3390/fluids4020104

Harkett J., Fletcher L. N., King O. R., et al. The thermal structure and composition of Jupiter's Great Red Spot from JWST/MIRI // Journal of Geophysical Research: Planets. — 2024. — Vol. 129, no. 10. — e2024JE008415. — https://doi.org/10.1029/2024je008415

Kida S. Motion of an elliptic vortex in a uniform shear flow // Journal of the Physical Society of Japan. — 1981. — Vol. 50, no. 10. — P. 3517–3520. — https://doi.org/10.1143/jpsj.50.3517

Larichev V. D. and Reznik G. M. On two-dimensional solitary Rossby waves // Doklady Akademii Nauk SSSR. — 1976. — Vol. 231, no. 5. — P. 1077–1079. — (In Russian).

Lemasquerier D., Facchini G., Favier B., et al. Remote determination of the shape of Jupiter's vortices from laboratory experiments // Nature Physics. — 2020. — Vol. 16, no. 6. — P. 695–700. — https://doi.org/10.1038/s41567-020-0833-9

Liu T., Wang B. and Choi D. S. Flow structures of Jupiter's Great Red Spot extracted by using optical flow method // Physics of Fluids. — 2012. — Vol. 24, no. 9. — P. 096601. — https://doi.org/10.1063/1.4752227

Marcus P. S. Numerical simulation of Jupiter's Great Red Spot // Nature. — 1988. — Vol. 331, no. 6158. — P. 693–696. — https://doi.org/10.1038/331693a0

McKiver W. J. The ellipsoidal vortex: A novel approach to geophysical turbulence // Advances in Mathematical Physics. — 2015. — Vol. 2015, no. 1. — P. 613683. — https://doi.org/10.1155/2015/613683

Meacham S. P. Quasigeostrophic, ellipsoidal vortices in a stratified fluid // Dynamics of Atmospheres and Oceans. — 1992. — Vol. 16, no. 3/4. — P. 189–223. — https://doi.org/10.1016/0377-0265(92)90007-g

Meacham S. P., Pankratov K. K., Shchepetkin A. F., et al. The interaction of ellipsoidal vortices with background shear flows in a stratified fluid // Dynamics of Atmospheres and Oceans. — 1994. — Vol. 21, no. 2/3. — P. 167–212. — https://doi.org/10.1016/0377-0265(94)90008-6

Nakamula A., Obuse K., Sawado N., et al. Stable solitary vortices in two-dimensional quasi-integrable systems // Journal of Physics: Conference Series. — 2023. — Vol. 2667, no. 1. — P. 012010. — https://doi.org/10.1088/1742-6596/2667/1/012010

Nezlin M. V. Baroclinic modification of the barotropic model of the large red spot of Jupiter // JETP Letters. — 1981. — Vol. 34, no. 2. — P. 77–80.

Parisi M., Kaspi Y., Galanti E., et al. The depth of Jupiter's Great Red Spot constrained by Juno gravity overflights // Science. — 2021. — Vol. 374, no. 6570. — P. 964–968. — https://doi.org/10.1126/science.abf1396

Petviashvili V. I. Red SPOT of Jupiter and the drift soliton in a plasma // JETP Letters. — 1980. — Vol. 32, no. 11. — P. 619–622.

Romanova N. N. Solitary Rossby waves in a baroclinic atmosphere // Izvestiya Akademii Nauk SSSR. Fizika Atmosfery i Okeana. — 1980. — Vol. 16, no. 7. — P. 675–682. — (In Russian).

Sada P. V., Beebe R. F. and Conrath B. J. Comparison of the structure and dynamics of Jupiter's Great Red Spot between the Voyager 1 and 2 encounters // Icarus. — 1996. — Vol. 119, no. 2. — P. 311–335. — https://doi.org/10.1006/icar.1996.0022

Sánchez-Lavega A., Hueso R., Eichstädt G., et al. The rich dynamics of Jupiter's great red spot from JunoCam: Juno images // The Astronomical Journal. — 2018. — Vol. 156, no. 4. — P. 162. — https://doi.org/10.3847/1538-3881/aada81

Shetty S. and Marcus P. S. Changes in Jupiter's Great Red Spot (1979-2006) and Oval BA (2000-2006) // Icarus. — 2010. — Vol. 210, no. 1. — P. 182–201. — https://doi.org/10.1016/j.icarus.2010.06.026

Simon A. A., Tabataba-Vakili F., Cosentino R., et al. Historical and contemporary trends in the size, drift, and color of Jupiter's Great Red Spot // The Astronomical Journal. — 2018. — Vol. 155, no. 4. — P. 151. — https://doi.org/10.3847/1538-3881/aaae01

Suetin B. P., Zhmur V. V. and Chkhetiani O. G. Baroclinic Model of Jupiter's Great Red Spot // Izvestiya, Atmospheric and Oceanic Physics. — 2023. — Vol. 59, no. 3. — P. 243–254. — https://doi.org/10.1134/s0001433823030088

Tikhonov A. N. and Samarskii A. A. Equations of Mathematical Physics. — Moscow : Nauka, 1977. — 736 p. — (In Russian).

Vasavada A. R., Ingersoll A. P., Banfield D., et al. Galileo imaging of Jupiter's atmosphere: The Great Red Spot, equatorial region, and white ovals // Icarus. — 1998. — Vol. 135, no. 1. — P. 265–275. — https://doi.org/10.1006/icar.1998.5984

Zhmur V. V. Mesoscale ocean eddies. — Moscow : GEOS, 2011. — 384 p. — (In Russian).

Zhmur V. V., Belonenko T. V., Novoselova E. V., et al. Application to the World Ocean of the theory of transformation of a mesoscale vortex into a submesoscale vortex filament when the vortex is elongated by an inhomogeneous barotropic flow // Oceanology. — 2023. — Vol. 63, no. 2. — P. 184–194. — https://doi.org/10.1134/s0001437023020157

Zhmur V. V. and Pankratov K. K. Dynamics of an ellipsoidal near-surface eddy in an inhomogeneous flow // Okeanologiya. — 1989. — Vol. 29, no. 2. — P. 205–211.

Zhmur V. V. and Shchepetkin A. F. Evolution of an ellipsoidal vortex in a stratified ocean in the f-plane approximation // Izvestiya of the Academy of Sciences of the USSR. Atmospheric and Oceanic Physics. — 1991. — Vol. 27, no. 5. — P. 337–346.